Numerical Simulation of the Nearshore Oil Behaviors Based on Computational Fluid Dynamics

Mohammadmehdi Raznahan

A Thesis

in the Department of

Building, Civil and Environmental Engineering

Presented in Partial Fulfillment of the Requirements

for the Degree of

Master of Applied Science (Civil Engineering) at

Concordia University

Montréal, Quebec, Canada

October 2020

CONCORDIA UNIVERSITY

SCHOOL OF GRADUATE STUDIES

This is to certify that the thesis prepared

By: *Mohammadmehdi Raznahan*

Entitled: *Numerical simulation of the nearshore oil behaviors based on Computational Fluid Dynamics*

and submitted in partial fulfillment of the requirements for the degree of

MASTER of SCIENCE (*Civil Engineering*)

Complies with the regulations of the University and meets the accepted standards with respect to originality and quality.

Signed by the final examining committee:

_____ Chair
Dr. Ahmed Soliman

_____ External Examiner
Dr. Ida Karimfazli

_____ Examiner
Dr. Liangzhu (Leon) Wang

_____ Supervisor
Dr. Chunjiang An

_____ Supervisor
Dr. S. Li

Approved by _____
Dr. Michelle Nokken, Graduate Program Director

_____2020 _____
Dr. Amir Asif, Dean
Gina Cody School of Engineering and Computer Science

ABSTRACT

Numerical Simulation of the Nearshore Oil Behaviors Based on Computational Fluid Dynamics

Mohammadmehdi Raznahan

Oil spills are a serious environmental problem. To better support risk assessment and pollution control for oil spills, a good understanding of oil transport in the environment is required. This information is essential for managing response priorities and preparing contingency and mitigating measures. This study focused on the numerical simulation of the nearshore oil behaviors based on computational fluid dynamics. Based on the Reynolds-averaged Navier-Stokes momentum equations for an incompressible viscous fluid and volume of fluid (VOF) method, a 3D numerical model of three-phase transient flow was developed.

It was found that the wave number, averaged flow velocity, and oil properties would affect the oil spread extent and the oil volume fraction for open water. The higher the averaged flow velocity and wave number, the lower the oil concentration, and the faster the oil's horizontal movement. The spilled oil may move to contact the seafloor by increasing the averaged flow velocity at the inlet boundary. By increasing the wave number, the oil would stay near the water surface. In nearshore, where the wave is the main seawater motion, the oil containment boom should be set preferentially to the direction of wave transmission for oil cleaning. It was also shown that by doubling the wave number and increasing the averaged flow velocity (ten times) simultaneously, the maximum oil volume fraction would be reduced by around 32%. Finally, it was found that water temperature had no significant impact on oil migration, and the impact of evaporation can be further considered in the future simulation.

In addition, this study showed that the presence of ice would make the spreading of spilled oil slower in horizontal direction because the ice can build natural barriers to oil movement. The higher the ice concentration, the slower spilled oil migrates in all directions, and the maximum oil volume fraction will vary by increasing the ice coverage on the water surface area. The wave frequency, the averaged flow velocity, and oil properties would affect the oil spread extent and the oil volume fraction. The dumping effect of the wave due to the presence of ice also makes the impact of this factor less critical than those in the open water.

ACKNOWLEDGMENTS

This research was supported by the Multi-Partner Research Initiative of Fisheries and Oceans Canada and the Natural Sciences and Engineering Research Council of Canada.

I would like to express my sincere gratitude to my supervisors, Dr. An and Dr. Li, for the continuous support of my study and research and their patience, motivation, and immense knowledge.

Finally, my deep and sincere gratitude to my beloved wife, Atefeh, for her unparalleled love, help, and support throughout my years of study and writing this thesis. This accomplishment would not have been possible without her.

TABLE OF CONTENTS

LIST OF TABLES

LIST OF FIGURES

LIST OF ABBREVIATIONS

6-DOF	Six Degree of Freedom
BL	Boundary layer
CFD	Computational Fluid Dynamic
COSIM	Chemical/Oil Spill Impact Model
CSF	Continuum Surface Force
DSD	Droplet Size Distribution
GNOME	General NOAA Operational Modeling Environment
MOBREC	Multi-Level Overtopping Break-Water for Energy Conversion
NWT	Numerical Wave Tank
OSCAR	Oil Spill Contingency and Response
OWEC	Overtopping Wave Energy Converters
OWM	Oil Weathering Model
RANS	Reynolds-Averaged-Navier-Stokes
SIMAP/OILMAP	Spill Impact Model Application Package/Oil Modeling Application Package
VOF	Volume of Fluid

CHAPTER 1. INTRODUCTION

1.1. Background

Oil spills are a frequent occurrence due to the widespread use of petroleum products and oil in everyday life (Chen et al., 2019; Zhu et al., 2020; Romero et al., 2017). The most massive oil spill because of an oil tanker accident was the Atlantic Empress in 1979 off Tobago's island in the West Indies, where 287,000 tonnes of oil were released after a collision with another vessel (Fingas, 2012). Spills and blowouts may occur during any offshore oil and gas exploration activity. For instance, from 1979 to 1998, 19821 wells were drilled in the Gulf of Mexico, which 118 wells resulting in uncontrolled blowouts (Fingas, 2012).

Spilled oil can cause significant damage to the environment (An et al., 2017; Cao et al., 2020; Spier, 2013). Spilled oil is a threat to marine life while floating at the surface and to shoreline creatures while it reaches by water waves and current (Hester, 2016). Marine mammal and bird species that must constantly pass through the air-water interface to breathe are especially vulnerable to oil exposure. Also, toxicity pathways in different species vary, including ingestion of oil, accumulation of contaminants in tissues, and mass death of eggs in fish (Chang et al. 2014).

The economic impacts are the second level of consequences. Oil spills can cause severe damage to fisheries. Physical contamination can disrupt business activities by fouling gear or blocking access to fishing sites. Marine-based industries such as port business, and sea-based transportation are also at risk from oil spills (Chang et al. 2014). The parties responsible for the spill are also committed to conducting response operations that satisfy all requirements set by regulations. A study on the possible economic impact of a spill on ocean-based industries conducted by the Fisheries Centre of the University of British Columbia predicts that a medium-sized spill requires $2.4 billion for cleanup costs (Hotte and Sumaila, 2012). Spills closer to shoreline have more significant economic impacts and are more expensive to clean. A study has estimated shoreline cleanup to be 4-5 times more costly than collecting the oil at sea (Nyman, 2009).

Societal impacts are the third level of consequences relating to the Oil Spill; it has negative implications on individuals' health and the well-being of communities. Webler and Lord (2010) noted that humans could be affected by oil spills in various ways, like health impacts from eating seafood with bioaccumulated oil toxins and health impacts from breathing oil vapors. Disruption

of recreational activities such as boating, swimming, angling, and diving caused by oil-contaminated shorelines is another social impact of oil spill.

Consequently, in order to alleviate the devastating impacts of spilled oil on the environment, economy, and society, research is needed to evaluate the various aspects of oil behaviors, specifically in the nearshore area. To better support the risk assessment and pollution control for oil spills at the shoreline and to effectively be prepared for response planning, it is required to have a good understanding of oil transport in the environment.

1.2. Specific Objectives

The objectives of this study are:

- To conduct a 3D simulation of wave propagation in shallow water with ANSYS Fluent and investigate the behaviors of spilled oil in the nearshore area to find out wave frequency to what extend affect the movement of spilled oil toward the seafloor in both open water and ice-covered waters. We will consider two wave numbers, one and two (k=1 and2), to change wave frequency.
- To investigate how many percentages of water surface area should be covered by ice pieces to cause a significant decrease in oil migration speed. Three different ice concentrations of 10%, 30%, and 50% are considered.
- To determine the effect of different average flow speeds at the inlet (0.1 m/s, 0.3 m/s, 0.5 m/s, and 1 m/s) on the maximum oil fraction and oil migration in x, y, and z directions.
- To show that different oil properties under the action of wave and water currents to what degree affect the fate and transport of spilled oil nearshore area.

1.3. Scope of the Work

To achieve the above-mentioned objectives, the rest of this thesis is designed as follows. Chapter 2 is the literature review, including the fate and transport of spilled oil, the process of spreading, oil spills models. Computational analysis of oil spills, which consists of numerical simulation of the submarine oil spill and computational analysis of oil spills in shallow water, will be discussed in this chapter. The next section would be the numerical simulation of the wave, study

of oil spills in ice-covered water, and summary of the literature review. Chapter 3 introduces methodologies and results of multiphase computational fluid dynamic (CFD) simulation of the nearshore spilled oil behavior in ice-free water. A discussion about the effect of the wave on nearshore oil behaviors, the effect of oil density and viscosity on nearshore oil behaviors, and the effect of water temperature on nearshore oil behaviors will be made. Chapter 4 shows methods and results for the simulation of spilled oil ice-covered seawater at the nearshore area. To what extend ice concentration, wave frequency, average flow velocity, and oil properties affect the maximum oil volume fraction, and spilled oil movement in a different direction will be discussed. Finally, Chapter 5 is the conclusion of this study, research achievements, and suggestions for future studies.

CHAPTER 2. LITERATURE REVIEW

2.1. Fate and Transport of Spilled Oil

Unexpected releases of oil over the years have ended in the pollution of the marine ecosystem. To better prepare for emergency response and alleviation of such oil spills, the fate and transport of different oil types should be predicated (Brandvik et al., 2006). Fate and transport of spilled oil is a complicated process. It is governed by evaporation, spreading, dispersion, emulsification, advection, photo-oxidation, dissolution, biodegradation, encapsulation, and sedimentation, which take place concurrently after an oil spill (Bobra and Fingas, 1986; Spaulding, 1988; Sebastiao and Guedes, 1995; Reed et al. 1999; Yang et al., 2015). Understanding the processes which are involved in the fate and transport of oil spills is key to good modeling, especially in improving emergency spill response models due to the fact that these models are used to predict where the spill will go (Anon., 2003). This knowledge is essential to manage response priorities (Anon., 2003), help make more beneficial predictions of the potential impact of petroleum-related developments, and prepare mitigating steps (Mackay and McAuliffe, 1988; Fingas, 2015).

Spreading

Spreading is once spilled oil, under the impact of gravitational, surface tension forces, viscous, and buoyancy, causes a thin slick to cover a vast area (Drozdowski et al., 2011). There are two dimensions to spreading: the thickness of the oil whereas it spreads and also the regional extent of the oil-contaminated zone (Vankatesh et al., 1990). The models used most for the spreading area unit supported the works that are done by Fay (1969) and Mackay et al. (1982). Fay (1969) indicated that spreading is best outlined in 3 phases – surface tension, inertial, and viscous. Gravity forces dominate the mechanical phenomenon part, the physical phenomenon part by physical phenomenon spreading, and also the vicious part by gravity and body forces. The model introduced by Fay has been subject to criticism for varied reasons. First, the water's body, not the oil, is utilized as a primary driving mechanism. Second, once the model is tested, it typically under-predicts spreading. This observation could also be understood partly because of horizontal diffusion ensuing from shear diffusion of waves (Elliott, 1986). one of Mackay's vital criticisms (Fay, 1969; Hoult, 1972) like formulations is that the spills area unit foretold to be circular in form,

with constant thickness notwithstanding what the wave and wind condition. Studies show that the spills area unit often thicker at the downwind finish and has shapes that area unit elongated (Galt and Overstreet, 2011; Reed et al., 1999).

Galt and Overstreet (2011) have projected an alternate formulation supported the observation that entrainment removes oil from the ocean surface, that's transported submerged in a very utterly sheared flow, which some a part of the spreading oil is coming to the surface owing to the buoyancy of rising oil droplets. During this methodology, breaking waves spread oil at the ocean surface is within the water column as oil droplets, with injection depths up to regarding one.5 times the breaking wave height. The oil driblet size distribution depends on the oil viscousness and also the breaking wave energy. The spread oil droplets rise back to the surface, looking at their size; the larger the droplets, the lot of accelerated the increase times. Currents within the higher water column area unit absolutely sheared thanks to wind and wave forcing of the near-surface layer. Droplets on the brink of the surface travel down-wind quicker than those at the most depth of penetration. These processes contribute to grease thickening at the forefront of the spill and a cutting at the edge. Galt and Overstreet (2011) have enforced his elementary strategy to regulate the standard modeling of spreading, mistreatment Delvigne and Sweeney's (1988) formulation for entrainment and their empirically-based oil driblet size distribution. It's necessary to notice that in Galt and Overstreet's formulation, oil driblet penetration depth is crucial to the entrainment formulation as this is often key to predicting the degree of thickening and cutting off oil.

Leibovich (1997) established a comprehensive numerical model for the interaction between wave and current based on earlier work (Leibovich, 1983). The computational burden for the model makes its regular use for practically prohibitive problems. Also, Galt and Overstreet (2011) have developed a simplified methodology with empirically modifying these model predictions. Galt and Overstreet's (2011) approach improves the current method since it explicitly analyzes an alternate way for spreading oil. Moreover, it can predict the observed thickening of oil at the downwind side of the spill. It merely plays a role in spreading if entrainment of oil is active, so it must supplement the existing spreading model. It needs work in the implementation and will require to be modified depending on the selected entrainment and droplet size models. Galt and Overstreet's (2011) method for dealing with transport associated with Langmuir cells is advancement and has never been achieved in a spill model. In the existence of steady winds,

surface wind stress and wave-induced (Stokes) drift can interact to create Langmuir cells. These cells arise in counter-rotating, helical vortex pairs aligned with the wind direction. The flows caused by the cells result in convergence zones at the sea surface and down welling between the cells. These cells are able for the broadly observed surface windrows. Oil is expanded in the convergence zones, and the down-welling may be adequately strong to entrain the oil. The presence of the cells improves the oil movement in the convergence zone at the surface down wind.

2.2. Oil Spill Models

The purpose of oil spill modeling is to predict where oil is possible to go after a spill (Afenyo et al., 2016). This is achieved by using data on ocean currents, waves, winds, and other environmental factors (Drozdowski et al., 2011). An oil spill model includes three main elements: the input, weathering, and transport algorithms to quantify the processes involved, and the output to appropriately produce the required outcomes (Sebastiao and Guedes, 1995; Yang et al., 2015; Spaulding, 1988).

Many studies have been dedicated to understanding and quantify how oil spills move on the water surface. As summarized in the comprehensive reviews of Spaulding (2017), and Afenyo et al. (2016), Response Model or OSCAR (oil spill contingency and response), (Reed et al., 2000), that is developed by SINTEF, Spill Impact Model Application Package/Oil Modeling Application Package or SIMAP/OILMAP (French McCay et al., 2015; Spaulding et al., 1992), GNOME/ADIOS (Lehr et al., 2000), GNOME (general NOAA operational modeling environment), (Zelenke et al., 2012), Chemical/Oil Spill Impact Model (COSIM) by Environmental Resource Management (Camp et al., 2010) address the three-dimensional surface and subsurface fate and transport processes and can be applied to both surface and subsurface releases. Also, Abascal et al. (2010) performed a study on the evolution of an analytical oil spill model and its validation. The oil slick observation during the Prestige accident was used to validate the results. The model has been implemented in the Bay of Biscay (Spain) to help spill response planning along the Cantabrian coast (Hānninen and Sassi., 2010; Abascal et al., 2010).

2.3. Computational Analysis of Oil Spills

Several researchers have conducted important tries to simulate the oil spill method with the assistance of CFD (Chao et al., 2001; Wang et al., 2005; Sayol et al., 2014). Chao et al. (2001) used a two-dimensional model. They divided the slick into many tiny grids, and every grid's properties, thanks to temperature change, spreading, evaporation, turbulent diffusion, and dissolution, were studied. This model expected the movement of the slick on the water surface. So as to simulate the distribution of oil particles within the water column, a three-dimensional oil fate model was developed supported the mass transport equation, and also, the concentration distribution of oil particles is often solved. Also, a comparison of numerical results with the determined knowledge was conducted and showed an honest agreement. Wang et al. (2005) developed a two-layer model for simulating oil spills in seas. This model thought of the oil in seas as consisting of the surface slick and suspended oil droplets entrained over the flow's depth. The model was supported by the particle methodology. The amount of oil released in the seas was distributed among a large number of particles tracked separately. They were driven by water current and wind-induced speed after they were on the water surface, and turbulent diffusion was additionally taken into consideration following a stochastic process approach.

The model includes several necessary processes: surface spreading, advection, emulsification, evaporation, dissolution, turbulent diffusion, the interaction of slick with the boundary, geological phenomenon, and also the temporal changes of physical phenomenon, oil body, and oil density. Sayol et al. (2014) have developed an associate degree, operational Lagrangian model, for following surface spills within the ocean. Contrary to most ancient Lagrangian particle tracking algorithms, this technique estimated the likelihood density function from the final position of a group of neutrally buoyant particles deployed within the flow providing the area of accumulated probability. The model departed from daily predictions of ocean surface currents, waves, associate degreed wind provided by an Operational statement System, and integrated the Eulerian velocities to get every particle's mechanical phenomenon forward in time. Also, a stochastic process term was accessorial to simulate numerical diffusivity. Varied tests were conducted to see the best numerical theme and also the procedure time step. So as to see the model's performance, the trajectories of a group of SVP-drifters deployed within the Balearic ocean were simulated. The drifters' final position set among the sculptured contour of fifty of the accumulated likelihood for the primary twenty-four h forecast.

Tkalich (2006) used a consistent Eulerian approach. The slick thickness was computed using layer-averaged Navier–Stokes equations. The advection-diffusion equation was applied to simulate oil dynamics in the water column. A high-order accuracy numerical scheme was developed to match the observed balance between diffusion, advection, and spreading phenomena. Vertical dynamics of oil droplets played a significant role in oil mass exchange between the water column and the slick. Oil mixing by breaking waves was parameterized by applying lately developed kinetic equations. The majority parameters of oil, water column, and breaking waves were combined into a single "mixing factor," quantifying partitioning of oil between the water column and the slick. The model could predict the oil entrainment rate for several dispersant application scenarios concerning storm intensity and duration. Governing equations were verified using test cases, data, and other models and consequently applied to Singapore Strait to simulate a theoretical oil spill.

Numerical simulation of submarine oil spill

In recent years, many studies have been done on oil leakage, which mainly focused on three aspects: calculation of oil droplet size distribution, underwater leakage characteristics investigation, and leakage location (Sun et al., 2019). A large number of studies has been carried out on oil droplet size distribution (Johansen et al., 2013; Nissanka and Yapa, 2016; Li et al., 2017; Cui et al., 2020). Many factors, such as dispersion, dissolution, breakup, and coalescence, are considered, which may significantly influence droplet size distribution. For the third aspect, researchers have conducted studies on the migration of spilled oil (Li et al., 2013; Zhu et al., 2014; Zhu et al., 2017; Sun et al., 2019).

Johansen et al. (2013) used a new methodology for the prediction of driblet size distributions from subsea oil and gas releases. The tactic was supported experimental knowledge collected from oil driblet breakup experiments conducted in a very new check facility at SINTEF. The ability was represented in a very companion paper, whereas this study addressed the theoretical basis for the model, and also, the empirical correlations had been wont to confirm the model parameters from the accessible knowledge from the check facility. The most issue addressed during this work was the idea for extrapolation of the information to full scale (blowout) conditions. Potential contributions from factors like buoyancy flux and gas void fraction were reviewed and assessed based on results from the DeepSpill field experiment.

In the study conducted by Nissanka and Yapa (2016), an improved model, Oildroplets, was introduced to calculate droplet size distribution (DSD) in underwater oil jets. The formulation by Bandara and Yapa (2011) was employed as the basic framework of the model. Theoretical changes were made in the coalescence closures and droplet breakup in order to enable the model to work in a wide variety of droplet sizes related to various release conditions. The evolution of oil droplets in a jet or plume was modeled using the population balance equation. Due to the droplet breakup and coalescence, death and birth were considered the model's source and sink terms. Due to turbulent pressure fluctuation and droplet coalescence due to turbulent fluctuations and different rise velocities, the droplet breakup was taken into account in calculating the DSD. Modified formulas for droplet collision rate, droplet breakup efficiency, and droplet coalescence efficiency were applied in the model. The model was verified using available field and recent laboratory experimental data. The model results corresponded well with the experimental data. The model accurately calculated the DSD for ultra-small droplet sizes as well as the relatively larger droplet sizes. The model showed a very good correlation for the middle droplet size with experimental data. Moreover, the model precisely calculated the dominant diameter range in all cases.

To assess the oil spill risk caused by accidental leakage of subsea pipelines, Li et al. (2017) developed a 3D, transient, mathematical model based on CFD to estimate the subsea oil release rate and simulate the oil dispersion behavior. The Eulerian-Eulerian approach was used to predict the subsea oil release rate, and the impact of hole size and ambient back pressure on the oil release rate was considered. The Eulerian-Lagrangian method was also used to track the migration trajectory of oil droplets from seafloor to sea surface. The oil dispersion behavior under different scenarios with different oil release rates, oil densities, current speeds, water depths, and leakage positions was taken into account. The actual case simulation application showed that the developed model is an alternative method for risk assessment and decision-making of unexpected leakage of subsea pipelines. Moreover, it was found that when the pipeline leakage occurs, a pressure drop will happen on the leakage point of the pipeline. Because the simulation approach considered the pressure drop, the simulation's oil release rates were lower than the values obtained by the classical formula. The hole size and ambient back pressure were the significant impact factors for estimating the subsea oil release rate. The oil release rate rose with the hole size increasing, while it reduced with the backpressure increasing. In this work, the oil movement under the current with actual shear speed distribution was also studied, and the oil dispersion behavior under different scenarios

(influence factors) was explored. In the scenarios simulation, the more rise time was needed by the situations with lower oil release rate, greater oil density, deeper water, leakage direction of upstream. The scenarios reached the longer horizontal migration distance with lower oil release rate, greater current speed, greater oil density, deeper water, or leakage direction of upstream.

Li et al. (2013) used the volume of fluid (VOF) model with a two-dimensional and three-phase flow numerical simulation of the submarine pipeline oil spill by FLUENT to forecast the trajectory of oil. The quantity and trajectory of spilled oil under some operating pressure, current velocities, and wave lengths were compared and analyzed. The simulation results showed that the operating pressure and current velocity are vital factors that affect oil spill behavior and incidence. They determine the position and area of surface oil films, which are very important for evaluating the oil spill behavior and incidence. The results indicated that wave and current have essential effects on the location and oil film area on the sea surface. The submarine diffusion scope of spilled oil was smaller with larger operating pressure or lower current velocity. With wavelength increasing, the water depth was influenced by waves. In the mentioned study, they only discussed two oceanic factors, wave, and current velocity.

The objective of the work has been done by Zhu et al. (2014) was to study the oil leakage from a damaged submarine pipeline with different leak sizes. CFD simulation with FLUENT software was conducted to investigate the process of an oil spill from a submarine pipeline to a free surface. They proposed a finite volume simulation combined with the VOF method. Impacts of oil leaking rate, oil density, leak size, and water velocity on the oil spill process were examined. The results showed that slow leaking, high density, small leak size, or fast current lead to a longer time for oil, reaching the maximum horizontal migrate distance when it reached the surface. Also, appropriate formulas were obtained to predict how to see oil reaching the sea surface. The formula for the dimensionless longest horizontal distance versus dimensionless density only met the polynomial; other formulas met the natural logarithm distribution. They indicated that using the formulas would be possible to obtain when and where oil reaches the sea surface and conduct rapid response. Finally, a model was proposed to forecast the maximum horizontal migration distance of oil at a particular time.

Zhu et al. (2017) investigated a numerical simulation on the underwater spread and surface drift of oil spilled from a submarine pipeline under the combined action of current and wave. The objective of this work was to evaluate the impacts of the physical ocean environment, spilled oil

density and viscosity, and leaking flux. The 2D Reynolds-Averaged-Navier-Stokes (RANS) equations, the VOF model, and the realizable k-ε turbulence model were utilized to solve the multiphase flow, and velocity-boundary wave-making technique combined with the sponge layer damping absorber technique realized the numerical wave flume. Oil spill experiments validated the numerical model. The calculation results indicated that under the wave's action, the spread of oil appeared more dispersed because of the oscillation of wave particles. However, the wave-particle velocity on the surface contributes to the increase in the drifting rate. Under this work's specific conditions, oil density has a noticeable impact on the underwater spread but restricted effect on the surface drifting. Low-density oil rose quickly, leaving a short time for response.

The purpose of the study by Sun et al. (2019) was to take the impacts of underwater spreading characteristics, wavelength, leakage direction, current speed, wind speed by using the VOF approach with a realizable k-ε turbulence model. The calculation results indicated that wavelength affects the underwater spread and drift process, while current speed and wind speed mainly influence the drift process. Leakage direction, oil density, and leaking rate had a significant influence on the underwater spread process but limited effect on the drift process. A formula was proposed to predict the oil diffusion distance at a particular time. The results of the investigation could be offered valuable guidance for the formulation of emergency response.

Computational analysis of oil spill in shallow water

Agrawal and Dakshinamoorthy (2011) proposed a detailed CFD based study to predict oil film's trajectory during different spill situations in shallow-water drilling. Three-dimensional simulations were carried out for various wave and current conditions. A three-phase flow, the VOF multiphase model, was used to capture the oil film's trajectory. A Fifth-Order Stokes theory described the seawater wave profile. The results indicated that ocean wave profile and current have essential impacts on the location and the extent of oil film on the sea surface. The polluted area increased with higher interaction of waves and current. At high wavelength, oil dispersion underwater increased, and the extent of oil film on the sea surface increased. Nevertheless, at high wave amplitude, the extent of oil film on the surface was reduced.

An oil spill model was applied by Sugioka et al. (1999) to simulate the fate of spilled oil. The Lagrangian discrete-parcel method was used in the model. The model has taken into account mechanical spreading, current advection, horizontal diffusion, dissolution, evaporation, and entrainment in simulating the oil slick movement. It calculated the sedimentation on the bottom

and the time evolution of the partition of spilled oil on the water surface. Also, a continuous source at a constant rate was set up as a tanker off the coast of Yokohama. The grid size was 1 km in the calculation domain. A 3-D hydraulic model was used to simulate the residual flow, and observed wind data were applied for advection. The simulated distribution of oil spreading agreed well with observations from satellite remote sensing.

2.4. Numerical Simulation of Wave

The water-waves is recognized as one of the most powerful sources of energy on the earth. According to the World Energy Council, the global wave power is likely at 2 TW. After ocean waves' formation, they can travel hundreds or thousands of kilometers across the ocean before reaching the shoreline (U.S Army Coastal Engineering Research Center, 1984).

With the succeeding developments in computational power and progress in graphics capabilities and 3D simulation, creating a CFD model and investigating results are substantially easier to get compared to experimental tests. This is reflected in lower operating time and, hence, in a low-cost analysis. Furthermore, this method brings excellent flexibility in the analysis types since it is somewhat easy to introduce or change dimensions and flow variables. Therefore, developing a Numerical Wave Tank (NWT) emerges to numerically model the wave behavior (Marques Machado et al., 2018).

Some authors have conducted researches involving numerical wave tanks. Clauss et al. (2005) studied the propagation of irregular waves by means of four commercial CFD programs: ANSYS CFX, ANSYS FLUENT, COMET, and WAVETUB. In their investigation, the first three programs, using the VOF method, were shown to be more precise in the simulation of the breaking of waves. Conversely, WAVETUB allows faster and more accurate analysis of wave propagation without breaking. In that situation, the wave propagation was modeled with the help of WAVETUB until the moment of the breaking. The results were showed a good agreement with experimental results. Nonetheless, it was found that all programs get higher wave heights than theory.

Lal and Elangovan (2008) used ANSYS CFX to validate a flap-type wavemaker. Various periods and strokes were set to the flap to understand the impact of these parameters on the generated waves' heights and lengths. Also, the waves' damping was investigated, taking into account the impact of the beach slope. Results involving the implementation of beaches with slopes

of 1:3 were proved to be the most effective in wave absorption. Also, different turbulence models were compared. Numerical simulations were performed using laminar flow, k − ε, and SST (Shear Stress Transport) models. No meaningful difference in results was detected. Silva et al. (2010) showed that ANSYS CFX gives precise results in regular wave generation simulation in intermediate depths. In that study, a flap-type wavemaker was adopted. The simulated results were analyzed with theoretical formulations (Linear theory and Stokes second-order theory). Those authors also investigated the influence of the domain height, computational mesh, and time step interval on the free surface elevation profile. Elangovan (2011) formed irregular waves using a flap-type wavemaker in ANSYS CFX. The results showed good compliance with the theory, showing that ANSYS CFX can be employed to model the generation of irregular waves. The author also investigated the impact of the beach slope on the absorption and reflection of waves. Finnegan and Goggins (2012) used ANSYS CFX to study linear waves in deep water. The waves were generated with a flap-type wavemaker, and several influence tests were conducted to optimize the numerical wave tank. The computational grid, the height, the time step interval, and the domain's length were the parameters optimized. The results were compared with the Linear theory, showing good agreement. The viscous effects were studied by performing simulations using the k – ε turbulence model. It was reported that the results do not vary from the laminar flow. Marques Machado et al. (2018) studied the generation and propagation of regular waves in shallow water by ANSYS CFX. Two different ways of making waves at the beginning of a numerical wave tank were tested, and it was found that the piston wavemaker provides more accurate results compared to the inlet velocity method. Also, the results showed a good agreement with Stokes second-order theory.

Generation of Regular waves was also the focus of Kh et al. (2017), who used numerical simulations to test the capability of two CFD software's ANSYS FLUENT and Flow 3D. A numerical wave tank with a flat bottom was created, and the authors concluded that comparing the index error between the simulations and the theoretical results, Flow 3D is the one that gives more accurate results. Their study also proved that ANSYS FLUENT is better for capturing the wave crest but presents a difference in the wave phase. Han et al. (2018) applied the numerical wave tank to study overtopping wave energy converters (OWEC). A multi-level Overtopping Breakwater for Energy Conversion (MOBREC) converter was applied at the tank's end. Using the ANSYS FLUENT program, regular waves were generated using a piston in order to study more

clearly its influence on the energy converter. Comparisons with experimental data have proven that ANSYS FLUENT gives correct results and that future work will be done to improve MOBREC. Tian et al. (2018) used ANSYS FLUENT to investigate the waves' impact interacting with a vertical cylinder in a 3D numerical wave tank. In order to verify the numerical simulation, regular waves were first generated and analyzed using a numerical wave tank with a flat bottom and without any structure inside. The waves were formed using the inlet-velocity method, and a damping zone was set at the end of the tank to prevent reflection. Compared with Stokes second-order theory, the results concluded that Ansys Fluent could precisely simulate the generation and propagation of regular waves. Also, Tian et al. (2018) studied wave-structure interaction on a vertical cylinder set in the numerical wave tank. The results of the wave, in this case, were compared with those with no cylinder in the numerical wave tank, and it was concluded that the maximum wave height decreases in the presence of the structure, but the wave phase remains equal. The results were in agreement with the theory but different from the experimental data. The authors argued that some factors of the measurement equipment could explain this experience.

2.5. Study of Oil Spills in Ice-Covered Water

During the last decades, human activities have been increased in the Arctic (Gjøsteen and Løset, 2004). Since human activity rises, there is a risk for marine oil spills in the region. This can be because of the rupture of pipelines, ship wreckage, either oil transported by tanker or bunker fuel oil. In the Arctic region, the presence of ice complicates understanding the behavior and fate of spilled oil. In response to this matter, some fields and laboratory studies have been conducted for modeling the behavior of oil spills in ice-covered water.

Oil spill models for ice-covered waters depends on those from open water with some modifications, by updating input parameters and employing oil in ice experiments (Afenyo et al., 2016). A recent review (French-McCay et al. 2017) showed little knowledge of oil spills modeling in ice-covered water than oil spills in open water. The SINTEF Oil Weathering Model (OWM), which is part of the Oil Spill Contingency and Response (OSCAR) model system, was modified with experimental and field outcomes from ice conditions (Brandvik and Faksness, 2009; Faksness et al., 2011). Data collected from the experiments were employed to calibrate the SINTEF Oil

Weathering Model (OWM) to predict oil spills' weathering in ice-covered waters (Brandvik and Faksness, 2009; Faksness et al., 2011).

When the oil is spilled, it is subjected to transport and weathering (Afenyo et al., 2016). It is moved by spreading, advection, dispersion, and sedimentation. In ice-covered water, encapsulation would be an additional process (Drozdowski et al., 2011). The fate and transport of spilled oil in the presence of ice are not completely different from that in ice-free water. Apart from the processes that are common to those in ice-free water, more complexity is seen when oil spills in snow, spill on, and under different ice types (Brandvik et al., 2006). The fate of spilled oil under the ice is affected by the ice bottom's roughness, ice concentration, ice cover size, droplet size distribution, melting and freezing (Beegle-Krause et al., 2013; Brandvik et al., 2006). Ice is pushed by the wind, which in turn drives the water. Also, Water currents may drive the ice. In both scenarios, the relative velocity between the water and the ice and the under-ice roughness determines the turbulence profile and, consequently, the oil droplet trajectories. Wind and waves may also lead to this process (Beegle-Krause et al., 2013). Under the bottom of smooth ice, oil flows freely and drifts quickly compared to oil in rough or ridged pack ice. A highly consolidated ice pack decreases energy due to the damping of waves (Beegle- Krause et al., 2013).

Yapa and Weerasuriya (1997) developed a numerical model to numerically simulate oil spreading under, though, and over a broken ice cover floating on calm water. The oil spreading under the broken ice cover was modeled by modifying the spreading equations for oil under solid ice. Oil seepage through the broken ice was considered as a simple, porous media flow. The oil spreading at the water surface near the top ice surface was modeled by considering the viscous forces and the interfacial tension. The transport processes were interconnected through mass conservation during numerical calculations. The results were compared with data from new experiments conducted in the mentioned study as well as experimental data. The presented model showed a good agreement with the observed data.

An experimental study was conducted by Izumiyama et al. (2002) at the ice tank of the National Maritime analysis Institute, Japan, to research the spreading behavior of oil spilled underneath ice covers. Tests were conducted for ice sheets with roughness on very cheap and level ice sheets with a flat bottom. Look at results for level ice sheets that showed an honest agreement with a theory that thought of the impacts of surface tension, engaged on the oil and oil body, and

buoyancy. Look at results for ice sheets with bottom roughness indicated that oil spreads during a smaller space; however, it will reach additional than underneath the grade ice sheet.

In experiments on oil spreading in broken ice conducted by Gjøsteen and Løset (2004), twenty tests were carried out. In each of them, oil was spilled on the water surface. Video cameras closely monitored oil spreading and flow motion, and the pictures were analyzed to find out the impacts of ice concentration, floe motion, slush concentration, and oil type on oil spreading. It was found that by increasing the ice concentration spreading rates would be decreased, but the result was negligible for ice concentrations below 20–30%. The slush presence strongly decreased the spreading so that the effect of changing the ice concentrations was reduced. Increased motion in the ice cover resulted in increased spreading rates, and this impact was especially pronounced in the presence of slush.

Li et al. (2013) simulated an oil spill in ice waters with the help of computational fluid dynamic software FLUENT. In that study, the nonlinear free surface boundary conditions were solved by the volume of the fluid model. The coupling of pressure and velocity under unsteady-state conditions was solved by pressure implicit with the operator algorithm's splitting. Moreover, the numerical wave water flume was set by the user-defined function with the help of C programming language. Based on this simulation method, the movement characteristics of the oil spill in ice waters were investigated. The results showed that: the oil adhered to the ice lower surface easily, while its diffusion area was less than the one on the free sea surface at the same temperature. Also, some oil was entrained to the ice upper surface and proceeded to move, which accelerated the ice melting; the pollution area caused by an oil spill near to the ice sheet was less than the one caused by an oil spill far from the ice sheet. The simulation results were validated by some experimental phenomena.

Boufadel et al. (2018) conducted a numerical investigation to determine how oil droplets transfer under the ice. It was found that the boundary layer (BL) in the water under ice creates a downward velocity that reaches up to 0.2% of the current speed in the horizontal direction, and this is larger than the rise velocity of 70 μm oil droplets. Also, the eddy diffusivity was increased with depth and decreased gradually afterward. By neglecting eddy diffusivity gradient when conducting Lagrangian transport of oil droplets, results would be in an unphysical spatial distribution. When the downward velocity of water was neglected, oil was stored at the water-ice

interface regardless of the attachment efficiency. The lift force was found to scrape off droplets of the ice, particularly for droplets $\leqslant 70$ μm.

2.6. Summary of Literature Review

Many studies have explored this topic in recent years in light of rising concerns about oil spills in the marine environment. Many studies have been dedicated to understanding and quantify oil spills models on the water surface. Also, several researchers have conducted significant attempts to simulate the process of the oil spill in deep water with the help of CFD, some focused on oil spills in shallow water. Moreover, many studies have been done on oil leakage, which mainly focused on three aspects: calculation of oil droplet size distribution, underwater leakage characteristics investigation, and leakage location. However, the number of researches that considers the oil spreading on the water surface under the action of wave and water current in the nearshore area is limited. Compared to the knowledge that exists for fate and transport of oil spills in Ice-free waters, knowledge regarding oil spills in ice-covered waters is more restricted, specifically, in shallow water. Some researchers have investigated the fate and transport of spilled oil in the presence of ice, the oil droplet transfer under the ice, and the impacts of ice concentration, floe motion, and oil type on oil spreading.

CHAPTER 3. MULTIPHASE CFD SIMULATION OF THE NEARSHORE SPILLED OIL BEHAVIOR IN ICE-FREE WATER[1]

3.1. Background

With the successive advancements in computational power and the progress in 3D manipulation of numerical models, modeling based on CFD has been widely used in the simulation (Kundu and Ghoshal, 2019). The CFD-based method is an alternative with lower operating time and cost, compared to large-scale experimental tests. Moreover, this approach has excellent versatility because it is relatively easy to introduce or modify some major parameters, such as dimensions and flow configurations. Studies of open channel flow, free-surface tracking, and numerical wave tanks have been reported recently (Fábio et al., 2018; Zhang and Li, 2017; Li and Li, 2020). Clauss et al. (2005) studied the propagation of irregular waves using four commercial CFD programs, ANSYS CFX®, ANSYS FLUENT®, COMET, and WAVETUB. In their analysis, the first three programs, using the VOF method, were found to be more accurate for modeling the breaking of waves (Fábio et al., 2018). WAVETUB enabled faster and more accurate simulation of wave propagation without breaking. However, it was found that all programs overpredicted wave heights. Silva et al. (2010) showed that CFX provided reliable outcomes in simulating regular waves' formation and propagation in intermediate depths. In their study, a flap-type wave-maker in CFX was used. The results showed good compliance with the theory, indicating that CFX has the potential to be used to model the formation of irregular waves.

The previous studies mainly focused on simulating regular waves in deep-water or simulation of oil leakage from submarine pipelines (Zhu et al., 2017; Sun et al., 2019).

[1] This chapter is a manuscript submitted for review by Environmental Pollution. “Multiphase CFD Simulation of the Nearshore Spilled Oil Behaviors” Mohammadmehdi Raznahan, Chunjiang An, S. Samuel Li, Xiaolong Geng.

Understanding the nearshore oil behaviors is essential for assessing oil spill risk for shorelines, and the fate and behaviour of the spilled oil will also impact spill response effectiveness. The current knowledge about the oil transport process in the nearshore areas is minimal. The fate and transport of spilled oil can be impacted by factors like waves and water current (Wei et al., 2013). Few studies have focused on the CFD simulation taking the wavy condition, shallow water, and impacts of environmental conditions into consideration. This study aims to conduct 3D simulations of wave propagation in shallow water and investigate the behaviors of spilled oil in the nearshore area under different conditions. The impacts of water currents, wave conditions, and water temperature on oil volume fraction and spilled oil distribution at the water surface will be explored.

3.2. Methodologies

3.2.1. Governing Equations

The governing equations are the Reynolds-averaged Navier-Stokes momentum equations and continuity equations, for a fluid which is incompressible and has a constant viscosity, given by

$$\frac{\partial \overline{u_i}}{\partial t} + \frac{\partial \overline{u_i u_j}}{\partial x_j} = -\frac{1}{\rho}\frac{\partial \bar{p}}{\partial x_i} + \nu \nabla^2 \overline{u_i} - \frac{\partial \overline{u_i' u_j'}}{\partial x_j} + g_i \tag{3-1}$$

$$\frac{\partial \overline{u_i}}{\partial x_i} = 0 \tag{3-2}$$

where $\bar{u}_i$ represents the Reynolds-averaged velocity component in the x_i-direction; u_i' is the velocity fluctuation in the x_i-direction; x_i is the space coordinate (i = 1, 2, 3); g_i is gravitational acceleration in the x_i-direction; t is time; p is pressure; ρ and ν are density and kinematic viscosity, respectively. For turbulence closure, the SST k−ω turbulence model was implemented, which was based on work of Devolder et al. (2018).

3.2.2. VOF with Surface Tension

A layer of air above the top of the water surface was taken into account, which is 50% of the domain's vertical dimension (2 m). Through considering some spilled oil near the water surface, the VOF method was adopted to track the position of spilled oil in this three-phase model (3 Eulerian phases, including air, water, and oil). In the VOF model, a single set of momentum equations was solved, and the volume fraction for each fluid throughout the domain was tracked.

The volume fraction of q[th] fluid in the computational cell is a_q. When $a_q = 0$, the cell is empty (no water or oil); when $a_q = 1$, the cell is full. When $0 < a_q < 1$, the cell contains interface between the q[th] fluid with either one or two other fluids. The tracking of interface(s) between phases was accomplished by satisfaction of the following equations:

$$\sum_{q=1}^{n} a_q = 1\,, q = 1,2,3 \tag{3-3}$$

$$\frac{\partial \mathrm{a_q}}{\partial \mathrm{t}} + \nu.\nabla \mathrm{a_q} = 0 \tag{3-4}$$

where ν is the averaged velocity vector of the cell. The subscript q = 1, 2, 3 denotes water, air, and oil phase, respectively.

The VOF model can include the impacts of surface tension along with the interface between each phase and the contact angles between the phases and the walls. For this purpose, the continuum surface force (CSF) model was implemented in this simulation, and the wall adhesion option was considered. These models are the work of Brackbill et al. (1992). The surface tension coefficient between oil and seawater were considered based on information from Environment and Climate Change Canada (Environment and Climate Change Canada, Oil Properties Database, 2001). The surface tension coefficient for oil/air and air/seawater came from Johansen (2002) and Gao et al. (2017), respectively.

3.2.3. Stokes Second-Order Wave Theory

For wave propagation, the Stokes second-order wave theory was applied as a boundary condition at the upstream side of the numerical wave tank. This wave theory is a nonlinear theory that describes regular progressive waves of finite amplitudes (Dean and Dalrymple, 1984). This theory gives expressions for the free surface profile and the velocity field. Based on this theory, the free surface profile of the wave is:

$$\eta = \frac{H}{2}\cos(kx - \sigma t) + \frac{H^2}{16}\frac{\cosh(kh)}{sinh^3(kh)}[2 + \cosh(2kh)]\cos[2(kx - \sigma t)] \tag{3-5}$$

with $\sigma = \sqrt{gk\tanh(kh)}$ (wave frequency);

$k = \frac{2\pi}{L}$ (wave number);

L as wavelength

where H is the wave height from crest to trough; h is the average water depth; x is the distance along the longitudinal direction.

The local velocity is given by:

$$u = -\frac{\partial \varphi}{\partial x} = \frac{H}{2}\frac{gk}{\sigma}\frac{cosh(kh+kz)}{cosh(kh)}cos(kx-\sigma t) + \frac{3}{16}\frac{H^2\,cosh(2kh+2kz)}{sin\,h^4(kh)}cos(2kx-2\sigma t) \quad (3\text{-}6)$$

$$w = -\frac{\partial \varphi}{\partial z} = \frac{H}{2}\frac{gk}{\sigma}\frac{\sinh(kh+kz)}{\cosh(kh)}\cos(kx-\sigma t) + \frac{3}{16}\frac{H^2\sinh(2kh+2kz)}{\sin h^4(kh)}\cos(2kx-2\sigma t) \quad (3\text{-}7)$$

where u and w are the velocity components in the longitudinal and vertical directions, respectively; z represents the vertical coordinate.

3.2.4. Geometry and Boundary Conditions

The geometry and detailed dimensions of the nearshore area in the present study are shown in Fig. 3.1. The surface water level is 1 m, and the thickness of the air layer above the sea level is 1 m. Wave parameters used in this study are based on the inlet velocity method, in which the averaged flow velocity and surface elevation of the waves are specified using the Stokes second-order wave theory equations. The wavelength, wave height, water depth, and steepness are 3 m, 0.15 m, 1 m, and 0.05, respectively. In order to further assess the impacts of wave frequency, two different frequency waves were simulated at the inlet of the numerical tank by assigning the wave numbers k to 1 and 2. Fig. 3.2 shows the wave propagation with two different wave numbers (k) at the inlet.

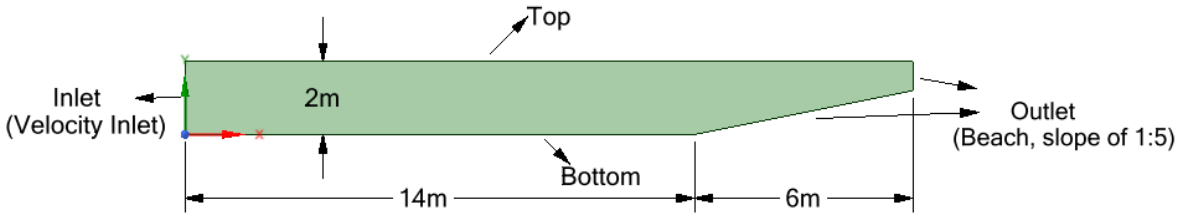

(a)

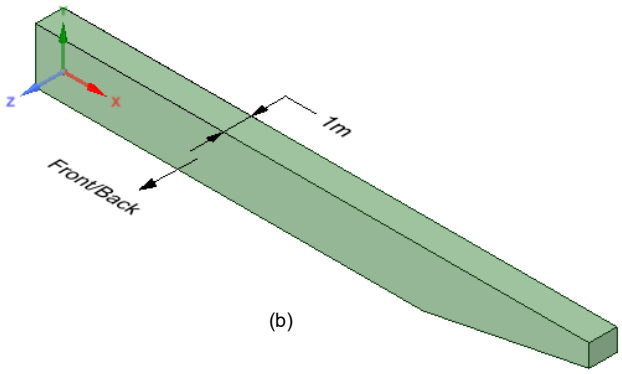

(b)

Fig. 3.1. Geometry of the CFD model domain for nearshore oil spill simulations: (a) elevation view; (b) 3D view. (x_1 and x; x_2 and y; x_3 and z are used interchangeably in this study.)

At the **Top** and the **Outlet** of geometry, pressure outlet with constant water surface of 1 m was considered. The remaining boundary conditions were set as follow (Fábio et al., 2018):

Bottom – A no slip wall was set to ensure an impermeable boundary at the bottom of the tank and the beach.

Front/ Back– Zero shear stresses in all directions were set.

The contact angle between all phases at the wall adhesion model was considered 90°.

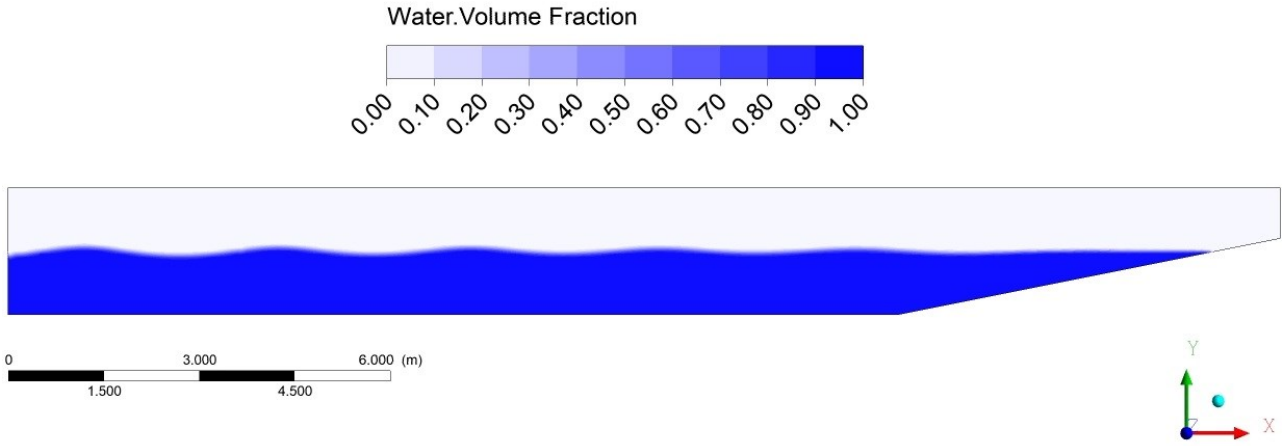

(a)

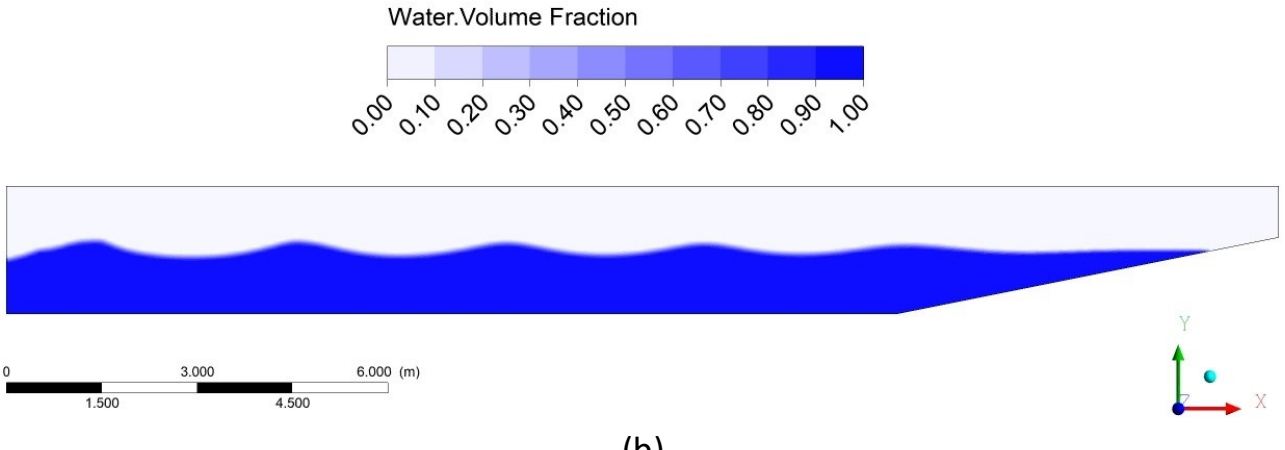

(b)

Fig. 3.2. Wave propagation after 18 seconds with k=1 (a) Wave propagation after 18 seconds with k=2 (b).

3.2.5. Initial Conditions

The conditions at t = 0 include the specification of the pressure field, velocity field, and volume fractions of each fluid. The velocity field and free surface location were initialized using Equations (3-5), (3-6), and (3-7). The pressure was assigned using hydrostatic values. Fig. 3.3 shows that the spilled oil volume was considered with the dimensions of 10×10×50 cm (length× height× width), and at a longitudinal distance of 50 cm from the inlet, near the water surface, and with the maximum oil volume fraction of 0.25. Hibernia, Hebron, Bunker C fuel oil, and Sable Island Condensate crude oils were used as the representative oils in this study. The average flow velocities at the inlet are 0.1 and 1 m/s.

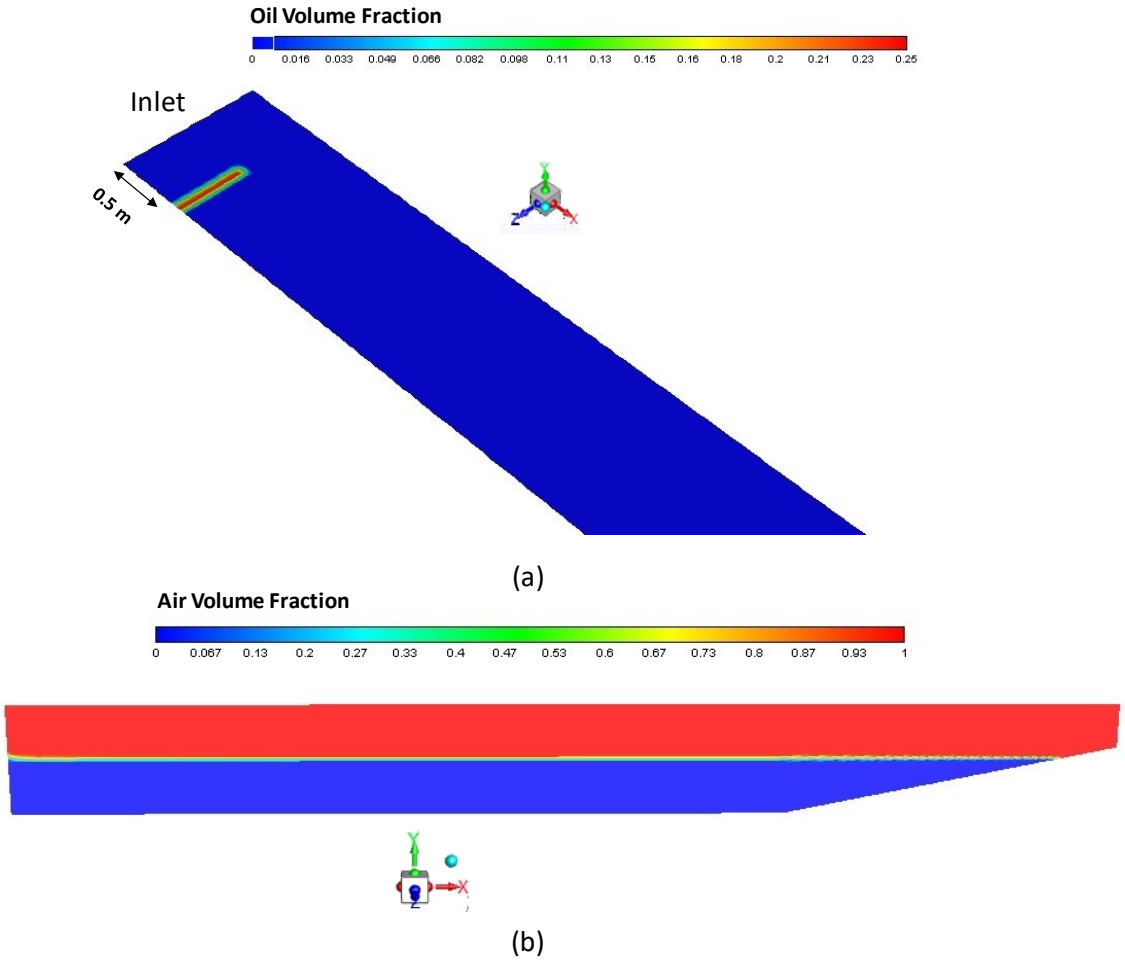

Fig. 3.3. Initial location and oil volume fraction of spilled oil at water surface, top view (a), and initial water surface level and air volume fraction, side view (b).

3.2.6. Computational Mesh

The computational mesh was created using ANSYS meshing. The size and type of mesh have an influence on the accuracy of numerical solutions to the governing equations; therefore, a suitable method should be used to create a structured mesh. In this study, the tetrahedrons method was first used, and then the steep gradients in the water-air interface were created with finer mesh resolution (Havn, 2011). Table 3.1 shows the mesh size parameters in this study.

It is assumed that Hibernia oil with an averaged velocity of 0.1 m/s moved at the water surface, and the maximum oil volume fraction, which is one of the main output in this study, was used to compare the grids. The relative error between mesh No. 2 and No. 3 was low, and mesh No.2 has fewer elements. To increase computing efficiency, mesh No. 2 was chosen as the main mesh size.

Table 3.1. Mesh size parameters

No.	**Mesh size (m)**	**No of elements**	**Maximum oil volume fraction (at the same location)**	**Relative error (%)**
1	0.045	1899930	0.051	7.8
2	0.04	2537858	0.055	1.89
3	0.03	4923075	0.056	

2.7. Simulation Parameters

The SIMPLE method and the second-order Stokes wave theory were adopted, as suggested by Finnegan and Goggins (2012) and Fabio et al., (2018). A 3D numerical model (open channel flow) with the three-phase flow in the transient mode was developed. Simulations were carried out using a transient approach with the second-order backward Euler scheme. Within each time step, a minimum residual of 10^{-4} was imposed. This is in accordance with the recommendation of Havn (2011) and Maguire (2011). In the present work, the time step intervals are 0.008 s, which is in agreement with the value suggested by Ning and Teng (2007). They recommended maximum

value of T/40, in which T is the wave period. Table 3.2 summarizes different model cases that were taken into account in this study.

Table 3.2. A summary of model cases.

Case No.	**Spilled oil**	**Averaged flow speed at the Inlet (m/s)**	**Wave number (k)**	**Water Temperature (°C)**
1	-	0.1	1	15
2	Hibernia	0.1	1	15
3	Hibernia	0.1	2	15
4	Hibernia	0.1	2	5
5	Hibernia	1.0	1	15
6	Hibernia	1.0	2	15
7	Hebron	0.1	1	15
8	Hebron	0.1	2	15
9	Hebron	1.0	1	15
10	Hebron	1.0	2	15
11	BunkerC Fuel Oil	0.1	1	15
12	SableIsland Condensate	0.1	1	15

3.3. Results and Discussion

3.3.1. Verification of the CFD Model

In order to verify CFD simulation, the surface elevation of waves was compared with the theoretical results given by the Stokes second-order theory. The surface elevation was defined at the initial instant for the entire domain based on the Stocks second-order theory. The comparison of the surface elevation of waves generated from the simulation at z = 1 m, t = 5, and 10 s with a water volume fraction of 0.3, with a theoretical surface elevation of waves is shown in Fig.3.4. As can be seen, the results showed good agreement with the analytical curve, with a maximum error of 4% in some points. The waves were very close in phase based on the theory. There was a small difference in the surface height, particularly at t = 10 s, when the last wave was in contact with the beach and affected some reflections in upstream waves. That might be due to coarse mesh or large time step interval. These results were also in agreement with those of Ning and Teng (2007) because of the similarity in size of time step interval. Based on obtained results, waves can be produced correctly, and it shows the good ability of this method in simulating the generation of progressive waves. Therefore, a film of spilled oil was considered on the water surface, which can be seen in Fig. 3.3, to investigate the impacts of water current and waves on oil volume fraction and oil distribution for different spilled oils. An analysis of the impacts of these factors will be conducted in the following sections of this work.

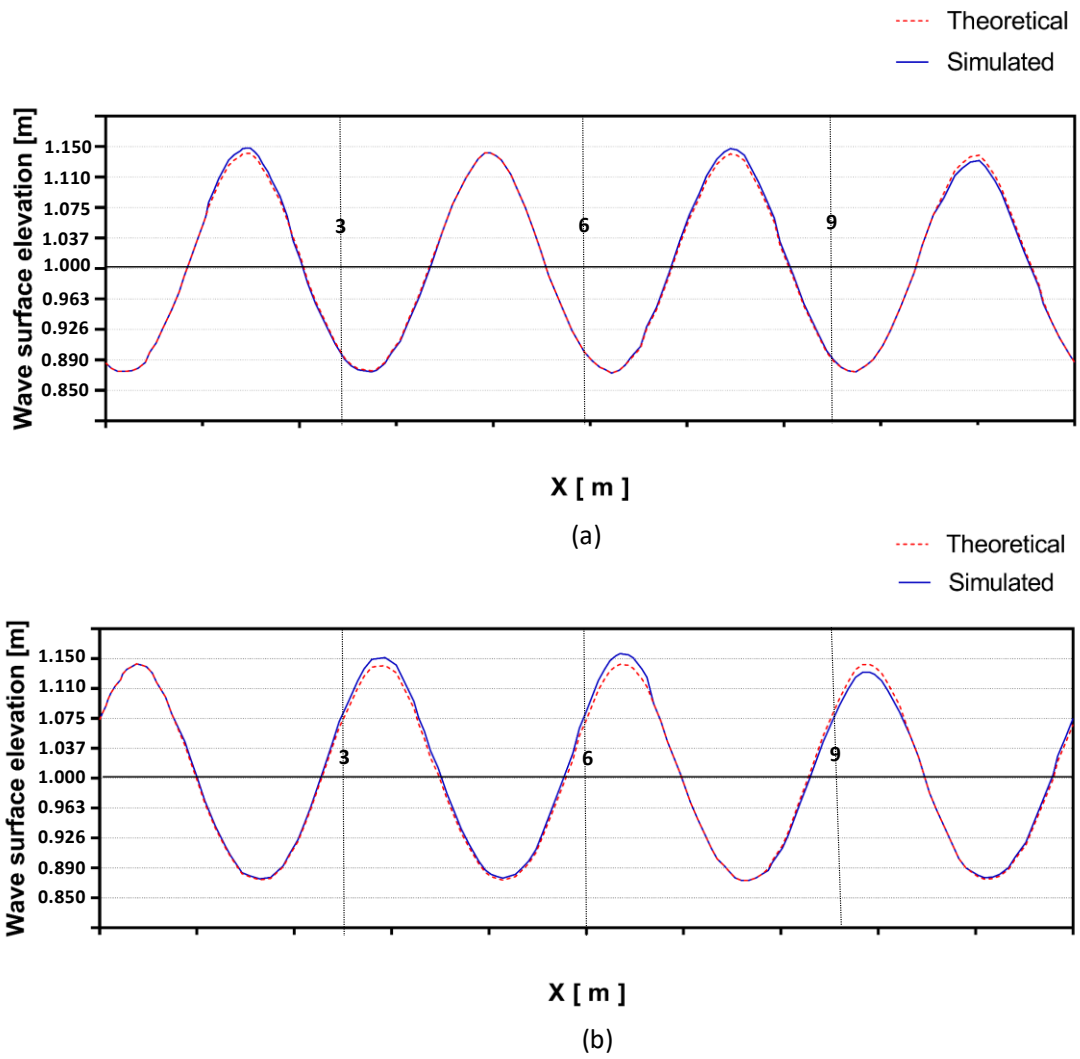

Fig. 3.4. Theoretical and simulated wave surface elevation at z = 1 m: (a) t = 5 s; (b) t = 10 s.

3.3.2. Effect of Averaged Flow Velocity on Nearshore Oil Behaviors

The spilled oil from an offshore pipeline leakage or other sources in seawater can reach the sea surface and become oil film. The averaged flow velocity plays an essential role in the migration of oil film in the nearshore area. In order to evaluate the effect of water current, a film of spilled oil on the water surface with a volume of 2500 cm3 was considered at t = 0 and at the distance of 0.5 m from the inlet, and the water temperature was 15 °C. Hibernia and Hebron oils were considered for this analysis. Since the density of spilled oil and seawater was almost the same, when the averaged flow velocity increased, there would be a more significant effect of the water

current on the oil migration in the *x*-direction. The reason is that a strong current could exert more shear stress on oil, leading to the transfer of more kinetic energy to oil. The maximum horizontal migration distances for u = 1 m/s after 18 s in a flow with k = 1 were 13.2 and 13.1 m for Hibernia and Hebron oils, respectively. The distances for u = 0.1 m/s were 3.9 and 3.8 m for Hibernia and Hebron oils, respectively. These results are in good agreement with those reported by Zhu et al. (2014 and 2017). When the averaged flow velocity was low (u = 0.1 m/s), as shown in Fig. 3.5 and Fig. 3.6, the current-driven oil movement was mainly in the y- and z-direction rather than the x-direction. The range of oil migration in the y-direction for u = 1 m/s after 18 s and with k = 1 was between 0.82 to 1.05 m and 0.82 to 1 m for Hibernia and Hebron oils, respectively, while the ranges for u = 0.1 m/s was 0.95 to 1.1 m for Hibernia and Hebron oils. By increasing the averaged flow velocity, the oil tended to spread less in the z-direction, as shown in Fig. 5 and Fig. 6. Therefore, the higher averaged flow velocity, the faster spilled-oil moving with sea current in the x-direction, and more oil migrating to the seafloor. At the same time, they will be more reluctant to migrate in the z-direction.

The maximum oil volume fraction will be reduced slightly by increasing the averaged flow velocity under the same wave condition. Fig. 3.5 and Fig. 3.6 show that at an increase of the water velocity by ten times for Hibernia and Hebron oils and with wave number equal to one (k = 1), after 18 seconds, the maximum oil volume fraction decreased by only 9%. Interestingly, when the wave number is two (k = 2), this reduced amount is negligible. The impacts of increasing water velocity on oil volume fraction at y = 1 m (initial water surface) after 18 s for Hibernia and Hebron are shown in Fig. 3.7 and Fig. 3.8, respectively. Consequently, the results indicate that the oil spread extent in the horizontal directions varies with the averaged flow velocity. If the averaged flow velocity is high enough, the spilled oil may move to contact the seafloor, resulting in more problems for oil control and recovery. The oil volume fraction would be reduced slightly by the averaged flow velocity, mainly when the wave number (k) was one.

3.3. Effect of Wave on Nearshore Oil Behaviors

To study the effect of waves on oil distribution and oil volume fraction, simulations were conducted by changing the wave number (k) for two different averaged flow velocity (u = 1 and 0.1 m/s) at 15 °C. Fig. 3.5 and Fig. 3.6 illustrate the effect of increasing wave number at different water velocity for Hibernia and Hebron oils, respectively. When the oil reaches shallow seawater,

they begin to move with water and diffuse to water horizontally (Wei et al., 2013). The effect of water on oil is more than buoyancy under the conditions of the sea wave. It means that by increasing the wave number, the oil will be more reluctant to move to the seafloor, and they tend to be floating on the water surface. The oil migration in the y-direction for u = 1 m/s after 18 s (wave number is two) was between 0.92 to 1.13 m and 0.93 m to 1.13 m for Hibernia and Hebron oils, respectively. These ranges with wave number of one (k = 1) were 0.82 to 1.07 m and 0.82 to 1 m for Hibernia and Hebron oils, respectively. However, the impact of increasing wave number on oil distribution in the z-direction was negligible. Under the same the averaged flow velocity, if the wave number increased, the oil would move faster in the horizontal direction (x-direction) of near-surface seawater. The maximum horizontal migration distances for u = 1 m/s after 18 s and with wave number of one (k = 1) were 13.2 m and 13.1 for Hibernia and Hebron oils, respectively. These values for u = 1 m/s and wave number of two (k=2) were 15.9 m and 15.85 m for Hibernia and Hebron oils, respectively. The wave particle velocity on the surface led to this increase in horizontal migration.

Increasing the wave number could contribute to a reduced-oil volume fraction while increasing the averaged flow velocity led to a small decrease in the oil volume fraction under the same averaged flow velocity. Fig. 3.5 and Fig. 3.6 illustrate that by doubling the wave number, the maximum oil volume fraction decreased by around 19% to 23% for Hibernia oil and 25% to 32% for Hebron oil after 18 s (for different current velocities). The main reason is that changing the wave number could result in lower surface tension in the oil; subsequently, the oil would be broken up more. The impact of increasing wave number on oil volume fraction at y = 1 m (initial water surface) after 18 s for Hibernia and Hebron oils are shown in Fig. 7 and Fig. 8. After increasing the wave number at a high-speed current (1 m/s), the oil volume fraction decreased suddenly, and it led to the breaking of oil. It can be found that the wave number plays a more crucial role than averaged flow velocity in decreasing the oil volume fraction.

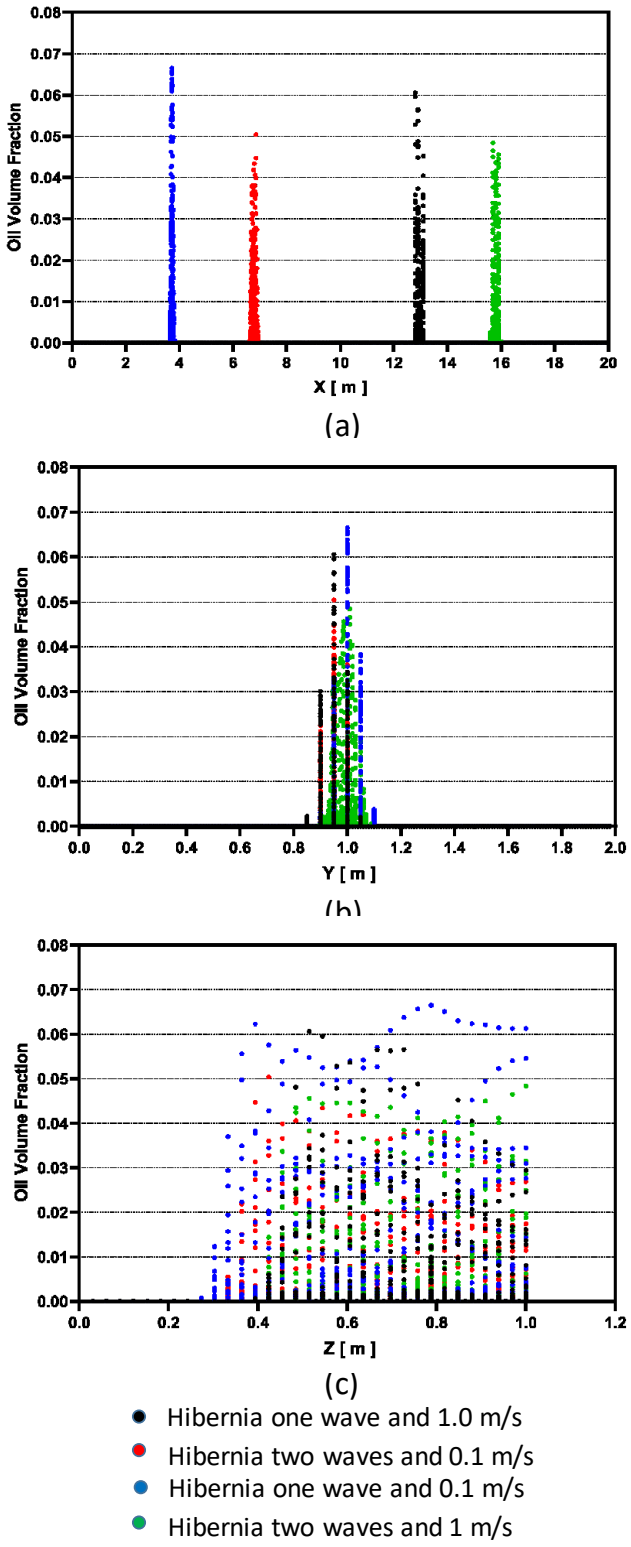

Fig. 3.5. Maximum oil volume fraction for Hibernia oil at t = 18 s: (a) x-direction (b) y-direction (c) z-direction

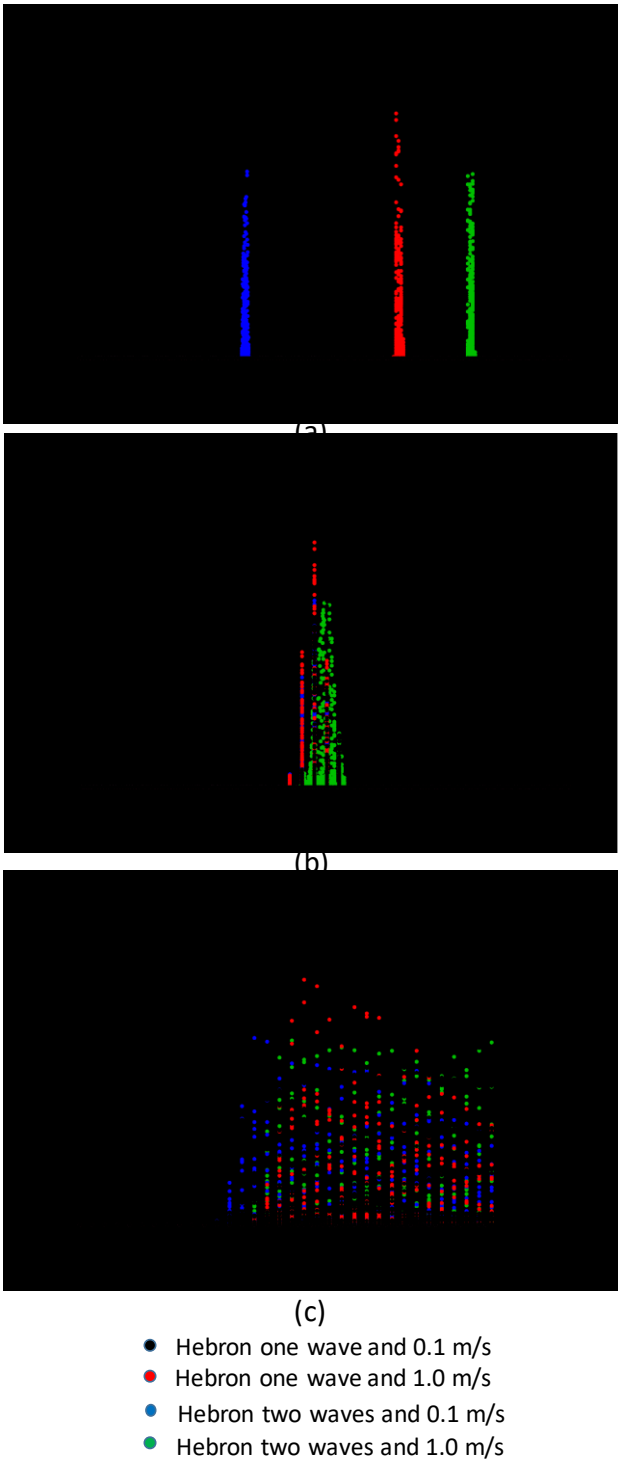

Fig. 3.6. Maximum oil volume fraction for Hebron oil at t = 18 s: (a) x-direction; (b) y-direction; (c) z-direction

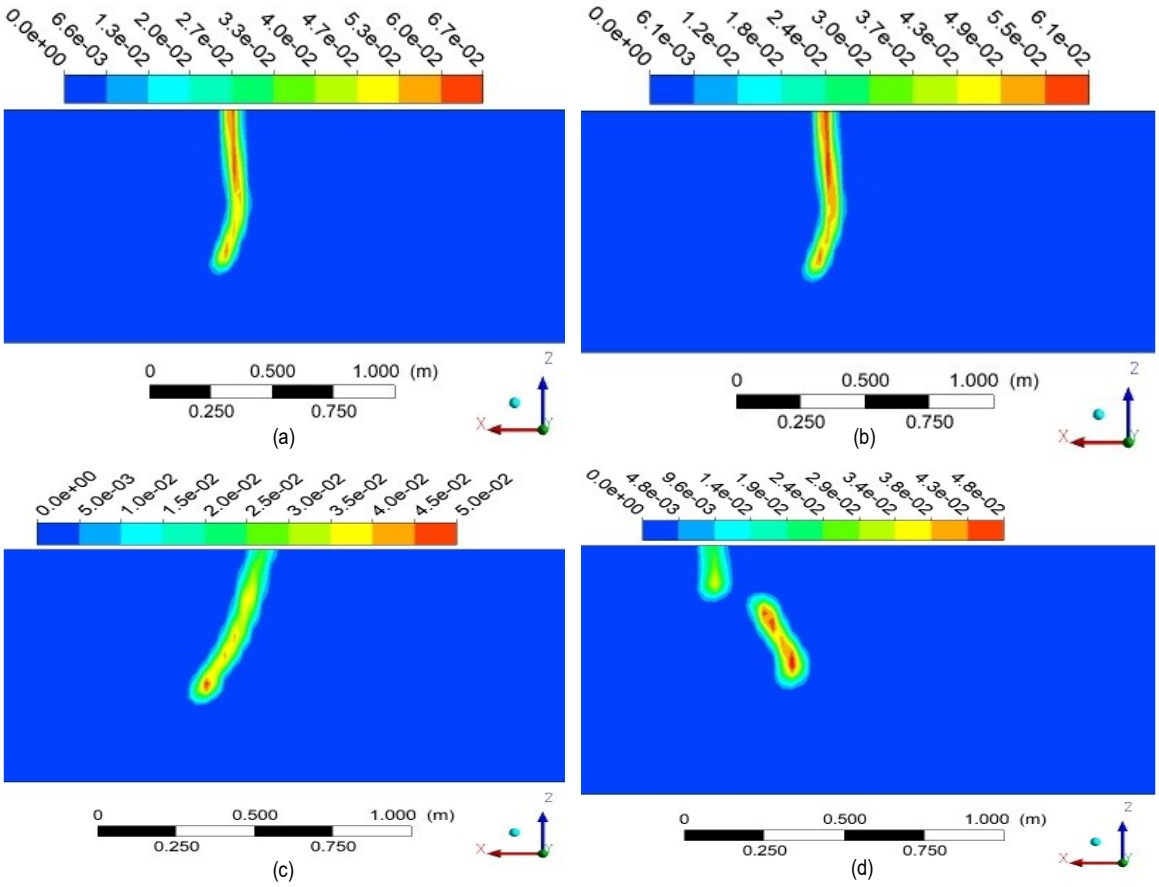

Fig. 3.7. Contour of oil volume fraction for Hibernia oil at t = 18 s, y = 1 m: (a) averaged flow velocity of 0.1 m/s and one wave; (b) averaged flow velocity of 1 m/s and one wave; (c) averaged flow velocity of 0.1 m/s and two waves; (d) averaged flow velocity of 1 m/s and two waves

Consequently, an environment where the averaged flow velocity and wave number are high enough (u = 1 m/s with k = 2) could effectively contribute to the reduction of spilled oil volume fraction in the nearshore area. However, the spilled oil spreads very quickly under superposition of higher wave number, and higher average flow velocity and fast responses would be required under this condition.

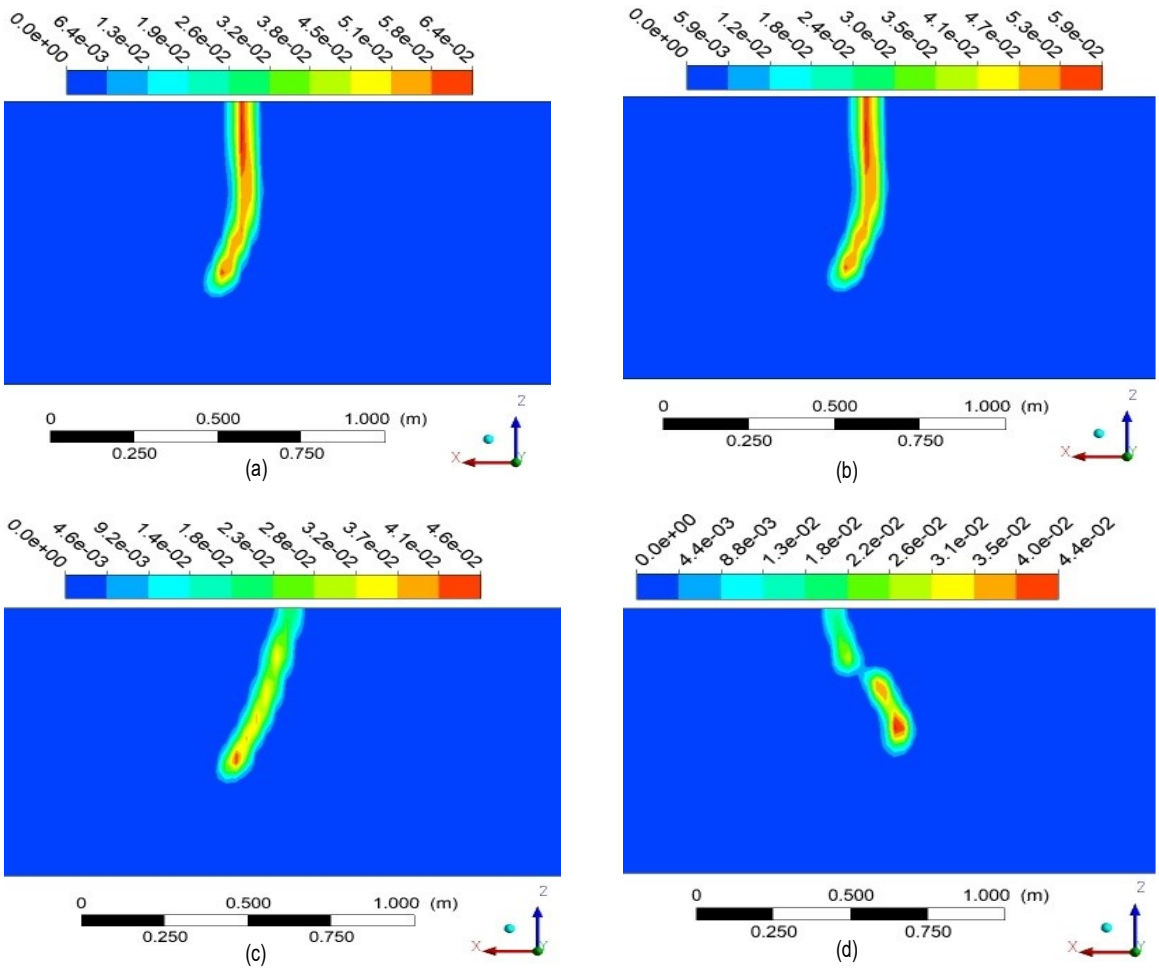

Fig. 3.8. Contour of oil volume fraction for Hebron oil at t = 18 s, y = 1 m: (a) averaged flow velocity of 0.1 m/s and one wave; (b) averaged flow velocity of 1 m/s and one wave; (c) averaged flow velocity of 0.1 m/s and two waves; (d) averaged flow velocity of 1 m/s and 2 waves.

3.3.4. Effect of Oil Density and Viscosity on Nearshore Oil Behaviors

Spilled crude oil-properties are among the most significant factors affecting the efficiency and effectiveness of oil spill response (Lee et al., 2015). The oil properties may vary to a considerable extent (Badiozamani et al., 2019; Pi et al., 2017). In this section, to study the effect of oil properties on the fate and transport of oil and oil volume fraction, simulations were conducted (u = 0.1 m/s and k = 1) by changing the oil type, which led to changing oil density, oil's dynamic viscosity and interfacial surface tension between oil and seawater while leaving other parameters the same. Four different oil types, including Bunker C, Hibernia, Hebron, and Sable

Island Condensate, were taken into account for the analysis. According to Environment and Climate Change Canada (Environment and Climate Change Canada, Oil Properties Database, 2001), Bunker C oil is a heavy oil (ρ = 969 g/mL at T = 15 °C) with a dynamic viscosity of μ = 45030 cP at T=15 °C,; Hibernia is a light oil (ρ = 839 g/mL at T = 15 °C) with a dynamic viscosity of μ = 49 cP at T = 15 °C; Hebron is a heavy oil (ρ = 930 g/mL at T = 15 °C) with a dynamic viscosity of μ = 585 cP at T = 15 °C; Sable Island Condensate is relatively a light oil (ρ = 875 g/ml at T = 15 °C) with a dynamic viscosity of μ = 2 cP at T = 15 °C.

Fig. 3.9 illustrates the process of oil migration in the horizontal, vertical, and lateral directions for the mentioned oils. It can be seen that the larger oil dynamic viscosity, the longer oil migration in the horizontal direction. While the oil density of Bunker C and Hebron is almost the same, the oil migration in the x-direction for Bunker C was around 40 cm longer than that for Hebron. Among other oils with similar dynamic viscosity, the movement of Hibernia oil in the x-direction was slightly faster than that for other oils, and this is due to the fact that the surface tension coefficient between Hibernia crude oil and seawater is higher than those for other oils. These results are different from those reported by Zhu et al. (2014), in which only different oil densities were considered for horizontal-migration evaluation.

Although a spill of oil is acted upon by different forces like gravity, buoyancy, viscous force, surface tension, the viscous force, and surface tension dominate, Bunker C oil's too high dynamic viscosity could strengthen the interfacial surface tension between the oil and water. That would lead to a relatively more extended migration of the oil with water current in the x-direction. Zhu et al. (2017) reported that the larger the oil density, the slower the oil migration in the x-direction. These different results might be because of the consideration of wave breaking and turbulence mixing in the present study.

The lateral migration of the oil was not affected by the changing oil dynamic viscosity and toil density. As shown in Fig. 3.9(c), the vertical migration of oil was affected by the dynamic viscosity of the oil. In the vertical direction, and oil was mainly subject to the force of buoyancy and gravity, and the higher oil density of Bunker C would increase the gravity of the oil. Nevertheless, the high dynamic viscosity of oil reduces the impact of gravity on oil.

The maximum oil volume fraction after 18 s and at y=1 m for these oils is shown in Fig. 3.10. It can be seen that the maximum oil volume fraction for Bunker C was almost 13% higher than those for Hibernia, Sable Island Condensate, and Hebron. Although their oil densities were

different, their maximum oil volume fractions were similar. This could be due to the high dynamic viscosity of Bunker C and high surface tension between oil and water. Consequently, the dynamic viscosity and surface tension of oil could play a more crucial role than oil density regarding the oil volume fraction.

3.3.5. Effect of Water Temperature on Nearshore Oil Behaviors

The temperatures of different regions are different and such difference can also impact the oil behaviors (Shrestha and Wang, 2020; Yao et al., 2020; Zhao et al., 2019). In this study, two water temperatures (15 and 5 °C) were considered to analyze the influence of water temperature on oil spreading characteristics and oil volume fraction. The influence of different water temperatures on horizontal, vertical, and lateral migration of spilled oil are shown in Fig. 3.11. It was found that changing water temperature did not result in a big variation in oil migration and oil volume fraction. One reason could be oil density, and oil dynamic viscosity would not change a lot at these two water temperatures, and because of considering constant surface tension coefficient between oil and air. The oil dynamic viscosity and surface tension are the most important parameters affecting the spilled oil migration. It should also be mentioned that there is an interrelationship among the chemical, physical, and biological processes that spilled oil undergoes, such as weathering of spilled oil through evaporation, emulsification, and dissolution (Ocean Studies Board and Marine Board, 2003). In many cases, evaporation is the most important process in terms of mass balance. The high temperature in seawater could lead to rapid evaporation, with the loss up to half of the volume of spilled oil. Such an effect of evaporation could not be considered in Fluent, and that is also a reason for not seeing significant changes in results with increasing water temperature. A comprehensive understanding of the impact of water temperature on spilled oil migration requires an accurate assessment of evaporation and emulsification.

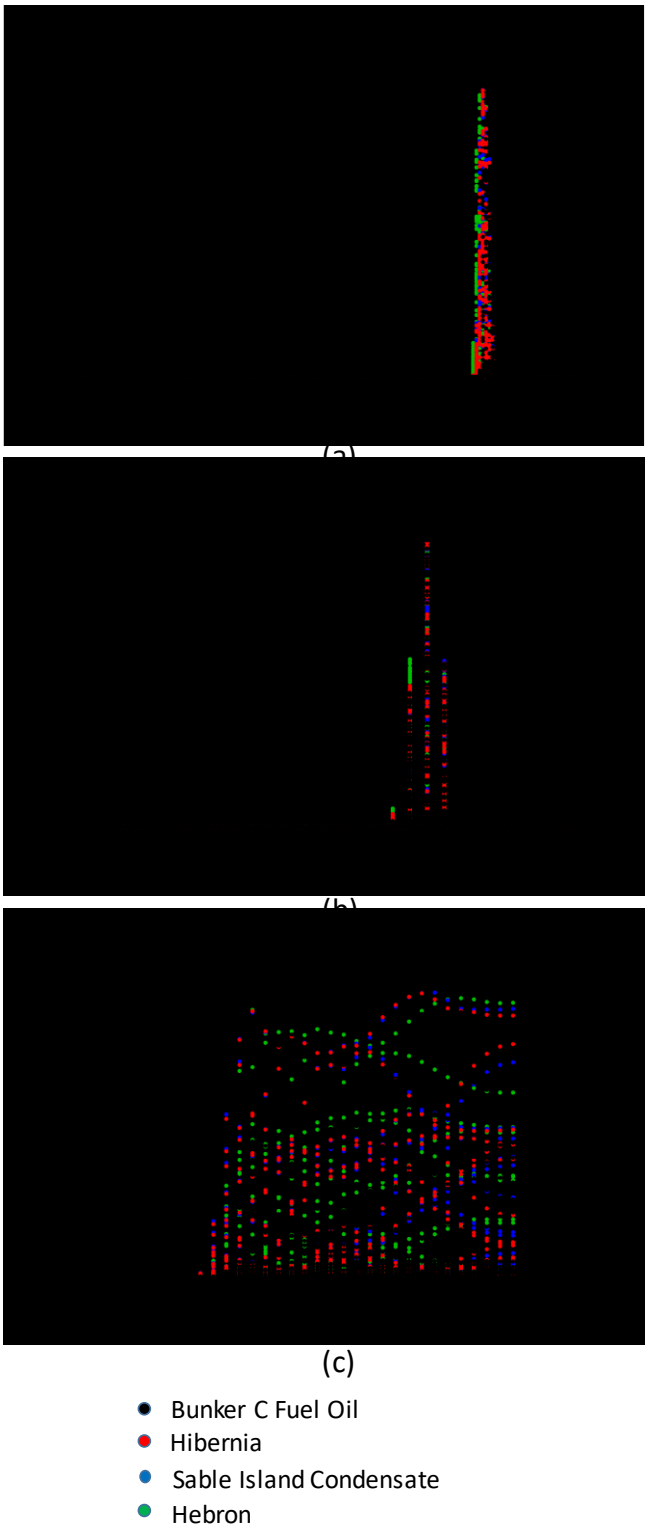

Fig. 3.9. Maximum oil volume fraction at t = 18 s, averaged flow velocity of 0.1 m/s and one wavenumber for different oils: (a) x-direction; (b) y-direction; (c) z-direction.

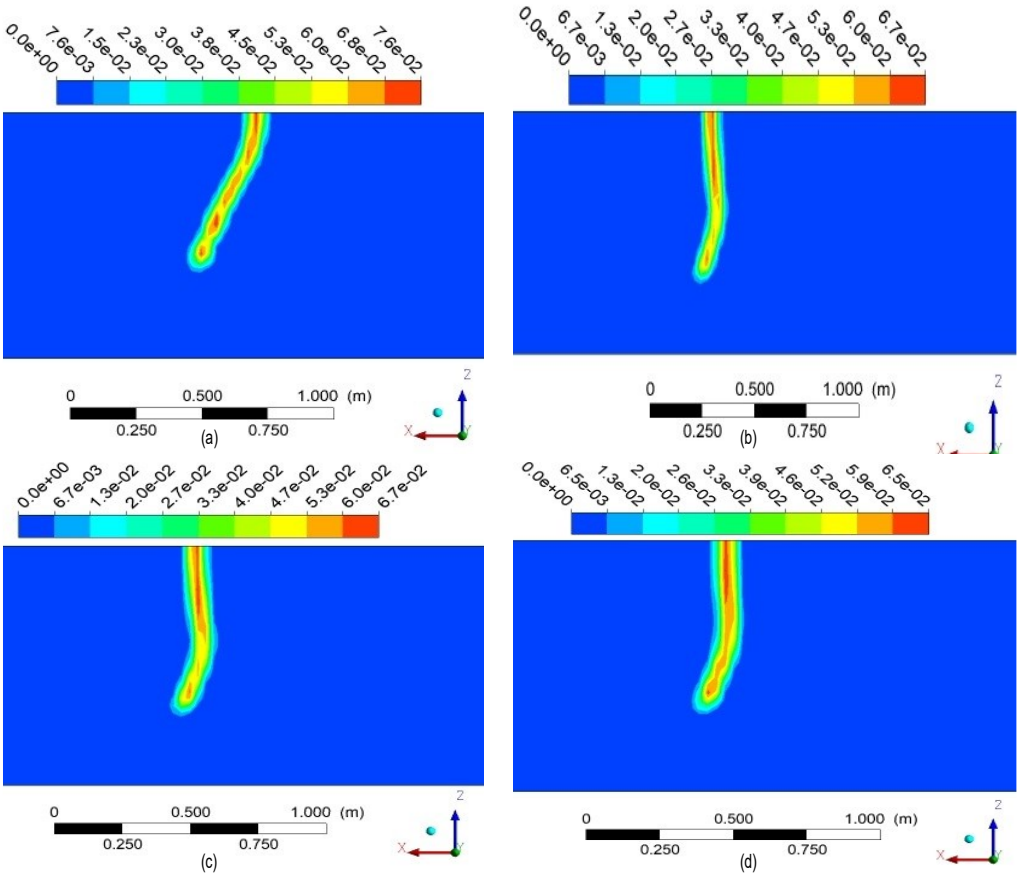

Fig. 3.10. Maximum oil volume fraction at t = 18 s, y = 1 m, averaged flow velocity of 0.1 m/s and one wave-number for different oils: (a) Bunker C Fuel; (b) Hibernia; (c) Sable Island Condensate; (d) Hebron.

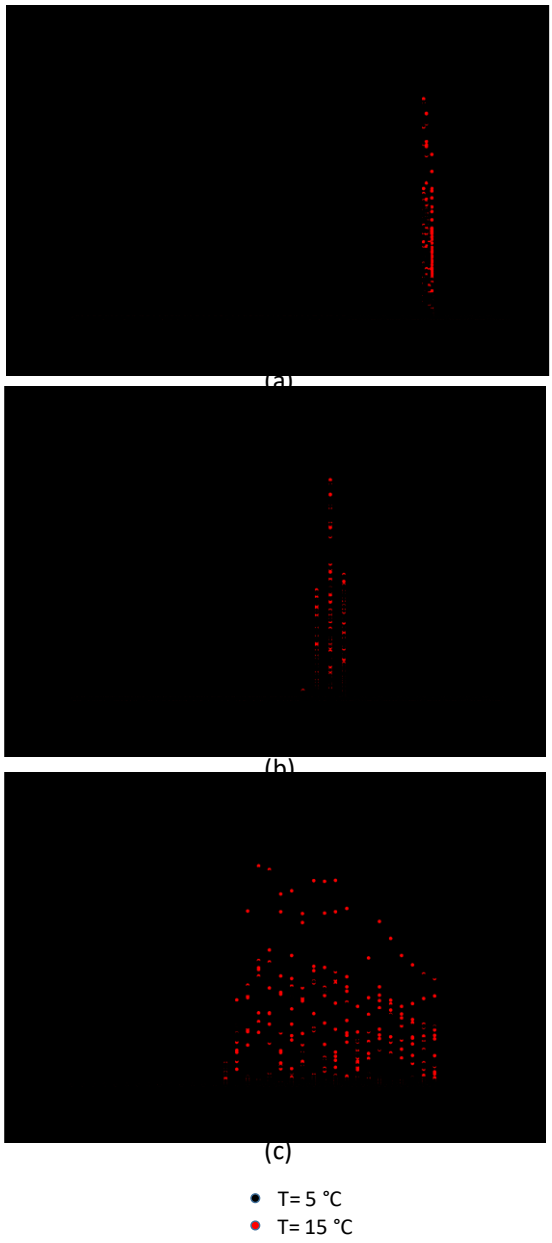

Fig. 3.11. Maximum oil volume fraction for Hibernia at T = 15 °C and 5 °C, at t = 18 s: (a) x-direction; (b) y-direction; (c) z-direction

3.4. Summary

In this study, oil behaviors in the nearshore area under the different wave and current velocities were investigated. Based on the Navier-Stokes equations for an incompressible viscous fluid and the VOF method, a 3D numerical model of the three-phase flow in the transient model was developed. It was found that the wave number, the averaged flow velocity, and oil properties would affect the oil spread extent and the oil volume fraction. The higher averaged flow velocity and wave number, the lower the oil concentration, and the faster the oil movement in the horizontal direction. The spilled oil may move to contact the seafloor when the averaged flow velocity is increased. By increasing the wave number, the oil would stay near the water surface. In nearshore, where the wave is the main seawater motion, the oil containment boom should be set preferentially to the direction of wave transmission for oil cleaning. It was also shown that by doubling the wave number and increasing the averaged flow velocity (ten times) at the same time, the maximum oil volume fraction would be reduced by around 32%, and it led to the breaking of oil. Finally, it was found that water temperature had no significant impact on oil migration, and the impact of evaporation should be considered in the simulation. The results of this study have important implications for understanding the oil transport and fate in the nearshore areas. That will help develop the appropriate strategy for the risk assessment and pollution control of spilled oil. The effects of some other environmental conditions can be further investigated in future studies.

CHAPTER 4. Multiphase CFD simulation of the Nearshore Spilled Oil Behavior in the Ice-Covered Water[2]

4.1. Background

Unexpected releases of oil in the last decades have resulted in the pollution of the marine environment (Afenyo et al., 2016; Chen et al., 2020). About 486,000 tonnes of crude oil was released at a water depth of 1520 m during the three months of the BP oil spill in the Gulf of Mexico (McNutt et al., 2011) and led to the pollution of 9900 km^2 of water surface (Wei et al., 2014).

Traffic in ice-prone environments has grown recently (Yumashev et al. 2017). Increased traffic may cause a growing risk from oil spills (Johansson et al., 2013). In response, to better prepare the mitigation of such spills, there is a need to predict the fate and transport of various oil types (Brandvik et al., 2006; Chen et al., 2021). Fate and transport of spilled oil is a complicated process, and the presence of ice makes it more complex. It is governed by evaporation, spreading, advection, emulsification, dispersion, dissolution, photo-oxidation, biodegradation, encapsulation, and sedimentation, which occur concurrently after an oil spill (Bobra and Fingas, 1986; Spaulding, 1988; Reed et al. 1999; Yang et al., 2015). Therefore, understanding the mentioned processes is key to good modeling, especially in developing emergency spill response models (Anon, 2003). These composite models are used to predict where and how the spill will go. This information is essential to determine response priorities, and help make better predictions of the potential impact of petroleum-related developments, and prepare mitigating measures (Anon., 2003; Mackay and McAuliffe, 1988; Fingas, 2015).

Compared to the knowledge regarding the fate and transport of oil spills in ice-free water, the knowledge that exists for oil spills in ice-covered waters is more restricted (French-McCay et al. 2017). Some general guidelines have developed, such as oil transport is practically unaffected

[2] This chapter is a manuscript to be submitted for review. ''Multiphase CFD Simulation of the Nearshore Spilled Oil Behaviors in Iced-covered waters'' Mohammadmehdi Raznahan, Chunjiang An*, S. Samuel Li, Xiaolong Geng.

by areal ice coverage when the coverage is less than 30%, and when the ice coverage is more than 70%, it becomes greatly affected (Reed et al. 1999; Li et al. 2016; French-McCay et al. 2017). Fingas and Hollebone (2003) showed that where oil was spilled (that is, under ice, on ice, under broken ice, under first-year ice, under multi-year ice, in pack ice, in leads, on snow, and absorbed into the snow) is a determinant of spreading in ice-covered waters. Since the ice can create natural barriers to oil movement, so the presence of ice floes or irregularities on and under the ice surface further delays the spreading of spilled oil (Evers et al., 2004); spilled oil may move several kilometers from where it was initially spilled if it gets encapsulated in ice or trapped under ice (Wilson and Mackay, 1987; Buist et al., 2013; Fingas, 2015). Yapa and Weerasriya (1997) developed relations for axis-symmetrical spreading and unidirectional spreading under broken ice in a study of spilled oil under broken ice.

Boufadel et al. (2018) conducted a numerical investigation to understand the transport of oil droplets under the ice. Li et al. (2013) simulated an oil spill in ice waters with the help of computational fluid dynamic software FLUENT. Based on this simulation method, the movement characteristics of the oil spill in ice waters were investigated. Few studies have focused on the CFD simulation taking the wavy condition in the presence of broken ice, with low ice concentration (less than 30%), nearshore area, and the impacts of environmental conditions into consideration. The goal of the current study is to simulate a 3D wave propagation in shallow water with different broken ice coverage to investigate the behaviors of spilled oil in the nearshore area under different conditions. The impacts of ice coverage, water currents, wave conditions, and oil properties on oil volume fraction and how spilled oil moves will be explored.

4.2. Methodologies

In the current study, the Ice pieces (Broken Ice) are treated as rigid bodies that are able to move freely in response to the waves and current. The problem is simulated by a fluid dynamics model (VOF model) coupled with the general equations of the rigid body motion (Six Degree of Freedom or 6-DOF).

4.2.1. Governing Equations for the Fluid Dynamic Model

The governing equations in the fluid dynamic model for a fluid which is incompressible and has a constant viscosity are the Reynolds-averaged Navier-Stokes momentum equations and continuity equations, which are given in Section 3.2.1 of Chapter 3.

4.2.2. VOF with Surface Tension

A layer of air over the water surface was considered, which is 50% of the domain's vertical dimension (2 m). Through considering some spilled oil at the water surface, the VOF method was adopted to track the position of spilled oil in this three-phase model (3 Eulerian phases, including air, water, and oil). The VOF model is discussed in Chapter 3 in detail (Section 3.2.2).

4.2.3. Dynamic Mesh Model and Six-degree-of-freedom (6-DOF) Solver

The dynamic mesh method can be applied to simulate the problem that the shape of the flow field varies with time due to the boundary motion. In order to describe the movement development of ice pieces in real-time, the boundary mesh of the computing domain should be dynamically updated for each time step. The volume mesh update was automatically handled by the FLUENT at each time step based on the ice pieces' new positions (Ansys Fluent Theory guide, 2013) The spring-based smoothing method, which is mainly based on the principle of spring approximation to control mesh deformation, and the local cell re-meshing method, which is mainly used to regenerate mesh in the calculation area, are applied in this study.

When ice pieces' motion creates the domain's adjustment, it is essential to know the fluid-dynamic loads acting on it in each time step. This makes it possible to measure the ice pieces' movement that defines the domain's new shape. This is the function of "six- degrees- of- freedom" (6DOF) (Ansys Fluent Theory guide, 2013). The governing equation for the translational motion of the center of gravity of the ice pieces is solved in the inertial coordinate system:

$$\dot{\overrightarrow{v_G}} = \frac{1}{m}\sum \overrightarrow{f_G} \tag{4-1}$$

$$\dot{\overrightarrow{\omega_B}} = I^{-1}\left(\sum \overrightarrow{M_B} - \overrightarrow{\omega_B} \times I\overrightarrow{\omega_B}\right) \tag{4-2}$$

where, $\overrightarrow{v_G}$ corresponds to the vectorial velocity ($\dot{\overrightarrow{v_G}}$ is the linear acceleration) of center of gravity. Also, m is the mass and $\overrightarrow{f_G}$ corresponds to each of the loads applied on the body of ice pieces, which may correspond to those generated by the flow.

On the other hand, the angular movement of ice piece is $\dot{\overrightarrow{\omega_B}}$, I is the inertia tensor, $\overrightarrow{M_B}$ is the moment vector applied to the body of ice piece and $\overrightarrow{\omega_B}$ corresponds to the angular velocity of the same. The angular and translational velocities are used in the dynamic mesh calculations to update the rigid body (ice pieces) position (Ansys Fluent Theory guide, 2013).

4.2.4. Stokes Second-Order Wave Theory

For wave propagation, the Stokes second-order wave theory was applied as a boundary condition at the upstream side of the numerical wave tank. This wave theory is explained in Section 3.2.3 of Chapter 3.

4.2.5. Geometry and Boundary Conditions

The geometry and detailed dimensions of the nearshore area in the present study are shown in Fig. 3.1. The surface water level is 1 m and the thickness of the air layer above the sea level is 1 m. Wave parameters used in this study are based on the inlet velocity method, in which the the averaged flow velocity and surface elevation of the waves are specified using the Stokes second-order wave theory equations. The wavelength, wave height, water depth and steepness are 5 m, 0.2 m, 1 m and 0.04, respectively. In order to further evaluate the effects of wave frequency, two different frequency waves were simulated at the inlet of the numerical tank, by assigning the wave numbers k to 1 and 2. Fig. 4.1 shows the wave propagation with two different wave numbers (k) at the inlet.

At the **Top** and the **Outlet** of geometry, pressure outlet with constant water surface of 1 m was considered.

The remaining boundary conditions were set as follow (Fábio et al., 2018):

Bottom – A no slip wall was set to ensure an impermeable boundary at the bottom of the tank and the beach.

Front/ Back– Zero shear stresses in all directions were set.

The contact angle between all phases at the wall adhesion model was considered 90°.

Three different average flow velocities at the inlet were considered in this study (0.1 m/s, 0.3 m/s, and 0.5m/s).

As it was mentioned previously, each ice piece was treated as a rigid body (Fig 4.2). The fate of oil trapped below the ice is affected by the roughness of the ice bottom, ice concentration, size of the ice cover, freezing, and melting (Beegle-Krause et al., 2013). Each ice's shape and dimension were considered based on work done by Gjøsteen and Løset, 2004. The ice thickness was about 5–6 cm, and the first ice piece was located at the 2-meter horizontal distance from the Inlet. Three different ice coverage percentage was taken into account in this study (10%, 30%, and 50% of water surface area). For each ice piece, a zero-shear stress boundary condition in all direction was set. For the ice wall roughness, sand-grain roughness height is considered based on Untersteiner and Badgley (1965), and Fingas and Hollebone (2003).

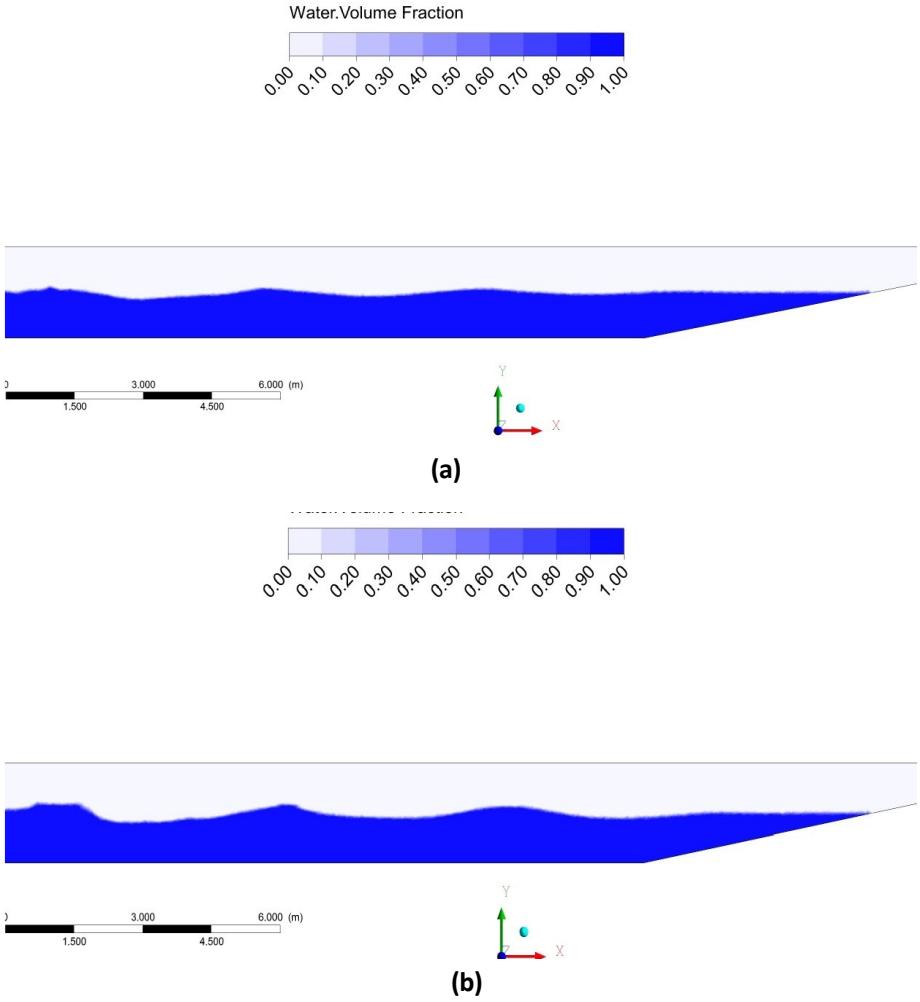

Fig. 4.1. Wave propagation after 18 seconds with k=1 (a) Wave propagation after 18 seconds with k=2 (b).

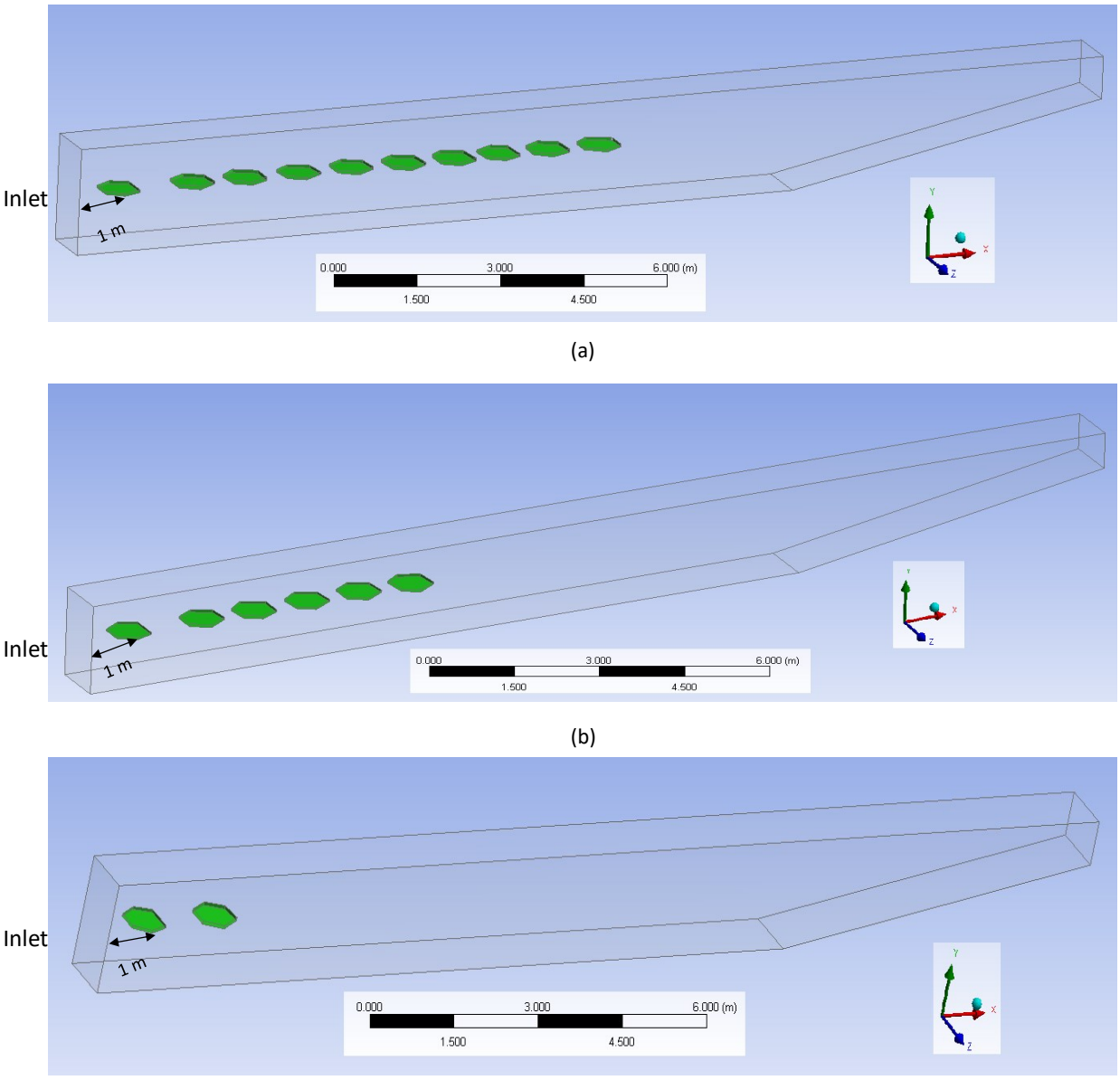

Fig. 4.2. Initial location of ice pieces; (a) 50% of the water surface area is covered by the broken ice. (b) 30% of the water surface area is covered by the broken ice. (c) 10% of the water surface area is covered by the broken ice.

4.2.6. Initial Conditions

The conditions at t = 0 includes the specification of the pressure field, velocity field and volume fractions of each fluid. The velocity field and free surface location were initialized using Equations (3-7), (3-8) and (3-9). The pressure was assigned using hydrostatic values. Fig. 4.3

shows that the spilled oil volume was considered with the dimensions of 10×3×50 cm (length× height× width), and at a longitudinal distance of 20 cm from the inlet, near the water surface, and with the maximum oil volume fraction of 0.25. Hibernia, Bunker C fuel oil, and Sable Island Condensate crude oils were used as the representative oils in this study.

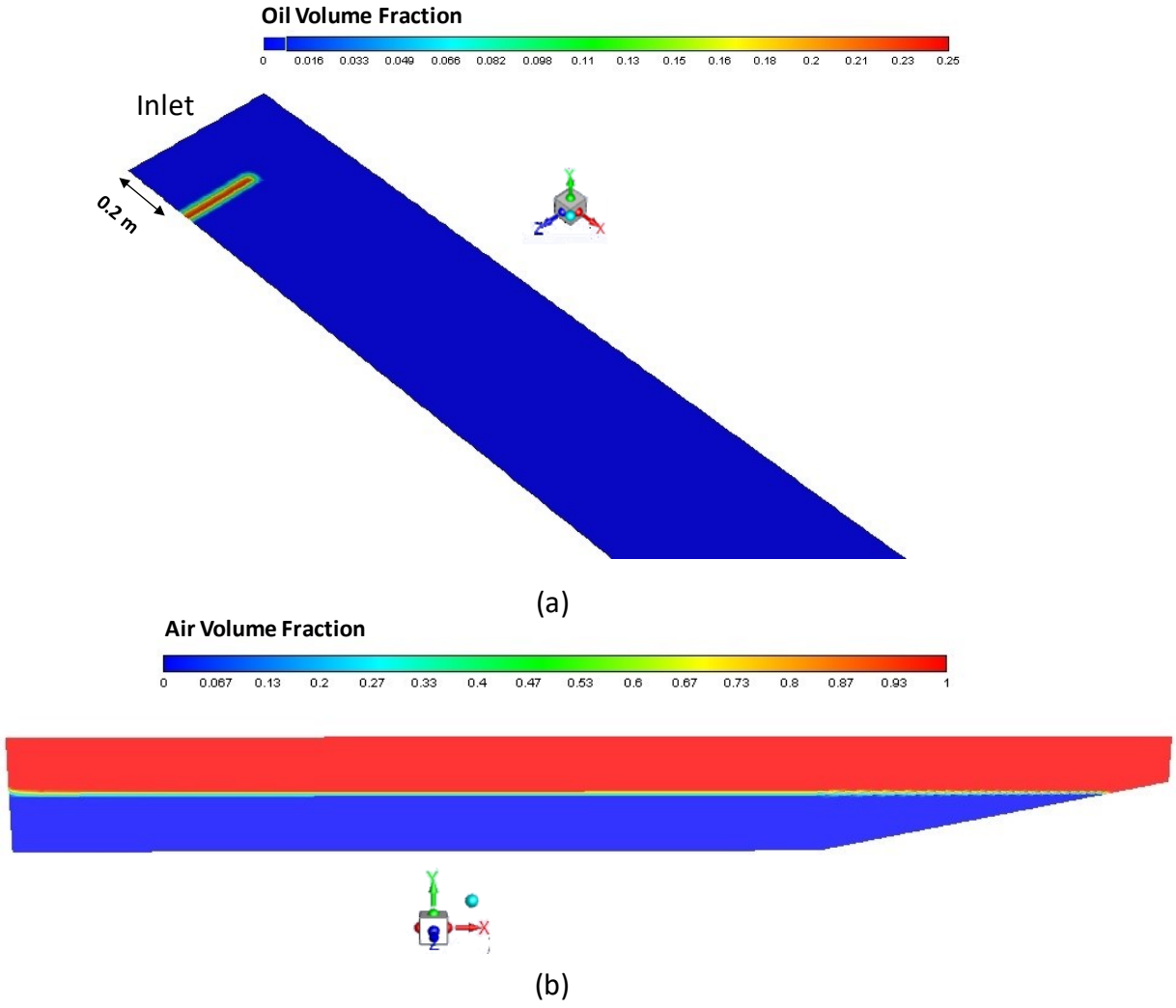

Fig. 4.3. Initial location and oil volume fraction of spilled oil at water surface, top view (a), and initial water surface level and air volume fraction, side view (b).

4.2.7. Computational Mesh

The computational mesh was created using ANSYS meshing. The size and type of mesh have influence on the accuracy of numerical solutions to the governing equations; therefore, a suitable method should be used to create a structured mesh. In this study, the tetrahedrons method was first used and then the steep gradients in the water-air interface were created with finer mesh resolution (Havn, 2011). Table 4.1 shows the mesh size parameters in this study.

It is assumed that Sable Island Condensate crude oil with an averaged velocity of 0.3 m/s at the inlet moving on the water surface, and the maximum oil volume fraction, which is one of the main output in this study, was used to compare the grids. The relative error between mesh No. 2 and No. 3 was low and mesh No. 2 has fewer elements. To increase the computing efficiency, mesh No. 2 was chosen as the main mesh size.

Table 4.1. Mesh size parameters

No.	**Mesh size (m)**	**No of elements**	**Maximum oil volume fraction (at the same location)**	**Relative error (%)**
1	0.045	3459822	0.041	9.7
2	0.04	4919700	0.045	2.2
3	0.03	11646861	0.046	

4.2.8. Simulation Parameters

The simulation parameters are exactly the same as those described in Chapter 3, Section 3.2.7. Table 4.2 summarizes different model cases that were taken into account in this study.

Table 4.2. A summary of model cases.

Case No.	Spilled oil	Averaged flow speed at the Inlet (m/s)	Wave number (k)	Ice coverage at the water surface area (%)
1	Sable Island Condensate	0.1	1	10
2	Sable Island Condensate	0.1	1	30
3	Sable Island Condensate	0.3	1	10
4	Sable Island Condensate	0.3	1	30
5	Sable Island Condensate	0.5	1	10
6	Sable Island Condensate	0.5	1	30
7	Sable Island Condensate	0.5	1	50
8	Sable Island Condensate	0.1	2	10
9	Sable Island Condensate	0.5	2	10
10	Sable Island Condensate	0.5	2	30
11	Sable Island Condensate	0.5	2	50
12	Hibernia	0.1	1	10
13	Hibernia	0.3	1	30
14	BunkerC Fuel Oil	0.1	1	10
15	BunkerC Fuel Oil	0.3	1	30
16	BunkerC Fuel Oil	0.1	2	10
17	Hibernia	0.1	2	10

4.3. Results and discussion

4.3.1. Verification of the CFD Model

To verify the CFD simulation, the surface elevation of waves was compared with the theoretical results given by the Stokes second-order theory. The surface elevation was defined at the initial instant for the entire domain based on the Stocks second-order theory. The comparison of surface elevation of waves is shown in Fig. 3.4.

4.3.2. Effect of Ice Coverage on Nearshore Oil Behavior

The presence of ice in open water has an impact on the fate and transport of oil (Brandvik et al., 2006). In order to evaluate the effect of ice coverage, a film of Sable Island Condensate oil on the water surface with a volume of 1500 cm3 was considered at t = 0, and at the distance of 0.2 m from the inlet and 0.3 m from the first ice piece, the water temperature was 5 °C, and 0.5 m/s was considered for the averaged flow velocity in this part of the study. Three different ice coverage percentages for the water surface area were considered, 10%, 30%, and 50%. Fig. 4.4 compares the spilled oil's transport in different ice coverage at the water surface when the wave number (k) is one and two. It was found that by keeping the wave number constant (i.e., a fixed oceanic forcing condition) and increasing the ice coverage at the water surface from 10% to 30%, the movement of oil plume in the x-direction decreases 10% to 15% depending on the wave number. As Fig. 4.4.d, 4.4.e, and 4.4.f demonstrate the transport of spilled oil with the wave number of one (k=1); when the broken ices cover 10% of the water surface area, the spilled oil reached more than a 12-meter distance from the inlet. The reduced-oil movement in x-direction could be explained by the fact that the lower ice surface's friction action leads to lower transport velocity of oil film than the free water surface. The increase in the ice coverage from 30% to 50% seems to have a negligible impact on the movement of oil in the x-direction; The maximum movement of oil plume in the x-direction for the flows with a similar wave number (k=1) and 30%-iced covered area and 50%-iced covered area are about 11.2 m and 10.6 m, respectively (Fig.4.5). Actually, the ice's presence makes some volume of the oil trapped under the ice moves toward the seabed. In the scenario when the wave number is two (Case No. 9, 10, and 11), the difference between the speed of oil spread in different ice coverage is remarkable. Spilled oil reached almost the beach area with the 10%-covered water surface area by ice and is still approximately 5 m and 6.2 m away from the beach area for scenarios where ice coverage is 30% and 50%, respectively. Fig.4.4 also shows that by increasing the ice coverage, the oil spread with more considerable variability. This variability is significantly reduced in the flow with 50% ice coverage on the water surface (Fig. 4.4.c and 4.4.f). It indicates that with relatively large ice coverage, the under-ice roughness could provide a major driving mechanism for the movement of spilled oil in the water.

For the transport of spilled oil in y and z-direction for flows with different ice coverage, Fig.4 5 demonstrates spilled oil behavior in detail. The majority of the spilled oil transport at the initial water surface (y= 0 m) in the different boundary conditions, but an increase of ice coverage makes the oil moves more toward the sea bed (Fig. 4.5.b., 4.5.e, 4.5.h, 4.5.k., 4.5.n., and 4.5.q.).

Interestingly, this transport of the oil volume toward the seabed would be increased dramatically when the wave number is two (k = 2). As can be seen in Fig.4.5.n and 4.5.q, when 50% or 30% of the water surface area is covered by ice and the wave number is two, some part of the oil volume moves at 0.2 m-distance of the seabed (y = -0.8 m). In the z-direction, while the broken ice's presence in the flow with the wave number of one does not cause a considerable difference in the lateral oil migration, decreasing the ice concentration in the flow with wave number of two makes the spilled oil increasingly more reluctant to transport laterally. As shown in Fig.4.5.o and 4.5.r, the oil film was spread in the z-direction from z = 0 m to z = 1 m.

Ice coverage affects the volume fraction of spilled oil in the water. Fig. 4.5 shows the volume fraction of spilled oil in x, y and, z-direction for different ice coverage with the wave number of one and two (k = 1 and 2). Our results indicate that the maximum oil volume fraction increased about two times as the ice coverage on the water surface area increased from 10% to 30% under the same flow condition. However, such behavior was not observed when the ice coverage in the water surface area increased from 30% to 50%, when k =1 (Case No. 5, 6, and 7), the maximum oil volume fraction with 50% ice concentration is 19% lower than those of flow with 30% ice concentration.

Compared to open water, our results demonstrate that the presence of ice generally reduces the spread of spilled oil in the x-direction, which is consistent with previous studies (Fingas and Hollebone, 2003; Evers et al., 2004; Brandvik et al., 2006). This is most likely because ice floes or irregularities under the ice surface create natural barriers that retard the spreading of spilled oil in the water. However, these results are not entirely compatible with those of Li et al. (2017) and French-McCay et al. (2017), indicated that oil transport practically unaffected by areal ice coverage when the coverage is<30%. Regarding the oil migration in the y-direction, the results showed that by the increasing presence of the ice from 10% to 30%, more volume of the oil trapped under the ice moves toward the sea bed, specifically for flows with k=2 (Case No.9,10, and 11). These results could be in agreement at some level with those of Gjøsteen and Løset (2004), due to the fact that although the aforementioned study was not comprehensive, the impact of wave did not consider in the analysis, the impact of ice concentration on oil migration in y-direction was investigated by keeping oceanic forcing condition the same in that study.

The current study also indicated that oil volume fraction and variability of oil spreading change with ice concentration. A decrease in the ice coverage greatly promotes the dilution of the spilled oil transport in x and y-directions.

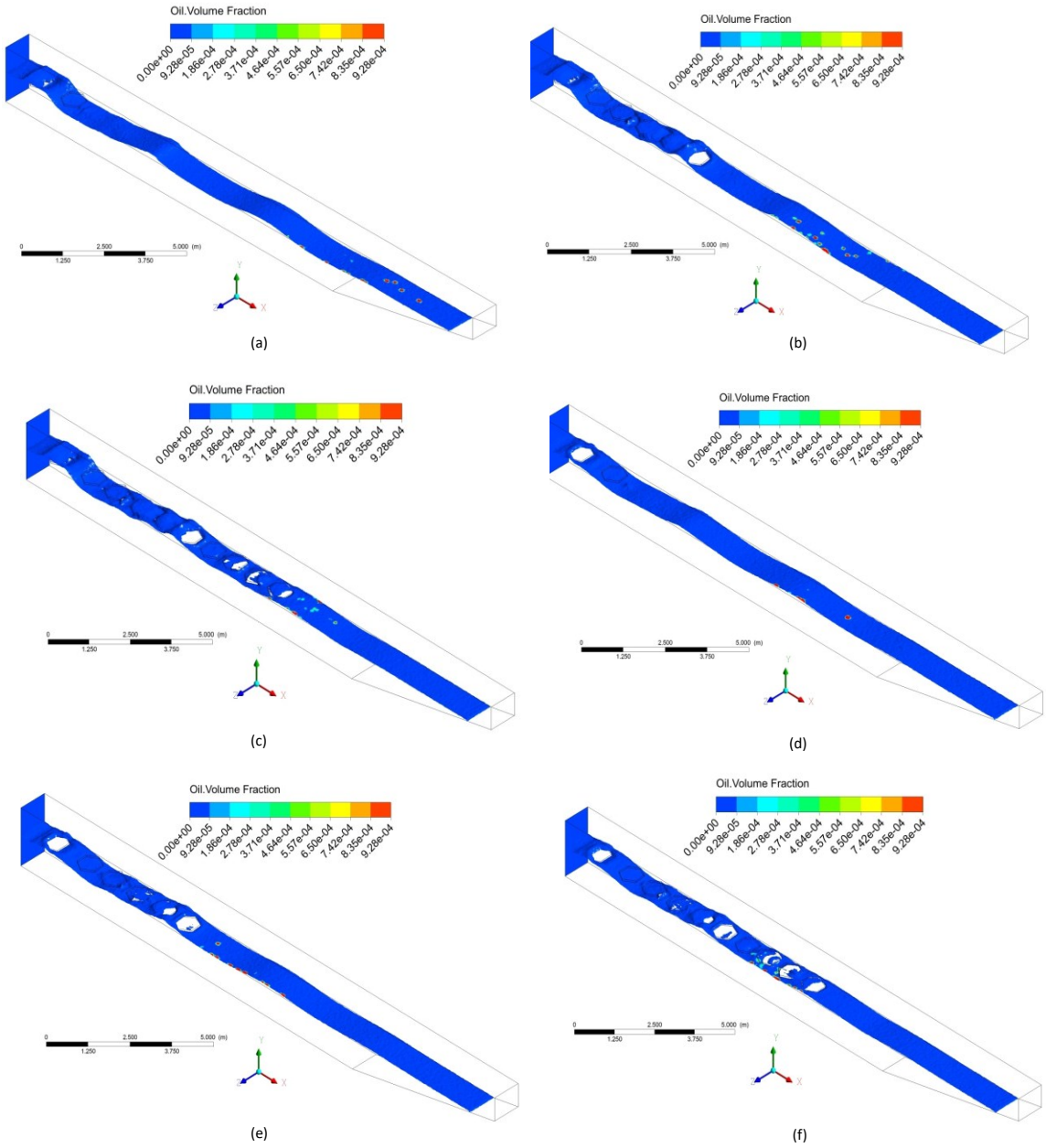

Fig. 4.4. Contour of oil volume fraction at the water surface for Sable Island Condensate oil at t = 18 s with the averaged flow velocity of 0.5 m/s: (a) the ice concentration is 10% and k = 2; (b) the ice concentration is 30% and k = 2; (c) the ice concentration is 50% and k = 2; (d) the ice concentration is 10% and k = 1; (e) the ice concentration is 30% and k = 1; (f) the ice concentration is 50% and k = 1.

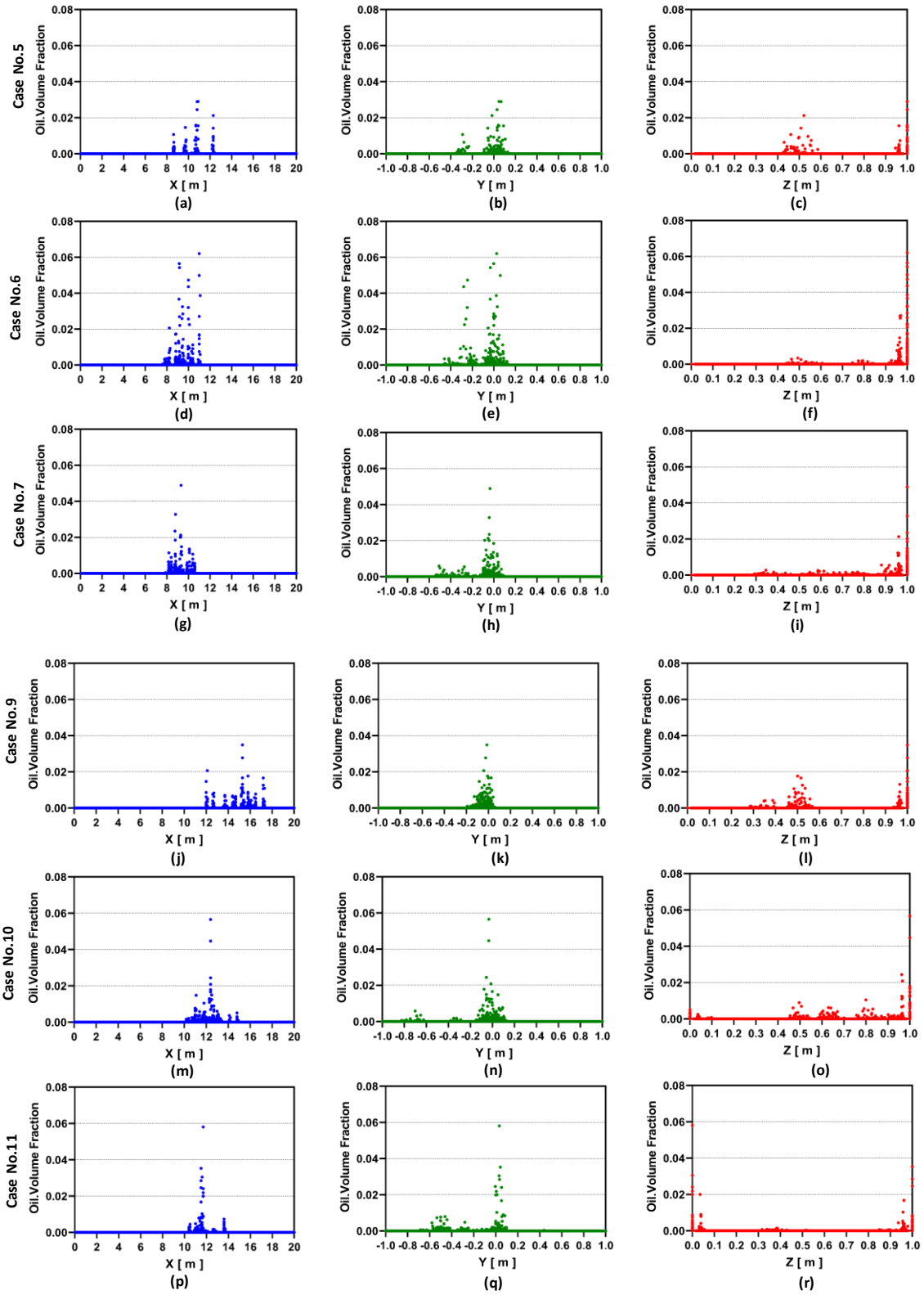

Fig. 4.5. Oil volume fraction of in x, y, and z-directions for different Case Numbers at t= 18 s, and constant average flow velocity.

4.3.3. Effect of Averaged Flow Velocity on Nearshore Oil Behavior

To study the effect of averaged flow velocity on spilled oil spreading behavior, a film of Sable Island Condensate oil was considered as the spilled oil. The water temperature was 5 °C, and the wave number is one (k= 1) in this part of the study. Three different average flow velocity at the inlet were taken into account, 0.1 m/s, 0.3 m/s, and 0.5 m/s. Spilled oil under the influence of viscous, gravitational, buoyancy, and surface tension forces between the phases spreads like a thin slick to cover a large water surface area (Drozdowski et al., 2011). Fig. 4.6 illustrates that when the averaged flow velocity increased, there would be a more significant effect of the water current on the oil migration in the *x*-direction. The maximum horizontal migration distances after 18 s in a flow with k = 1 and the ice concentration of 10% were 6.1 m, 8.9 m, and 12.2 m for the flow with for u = 0.1 m/s, u = 0.3 m/s, and for u = 0.5 m/s, respectively. In the situation when 30% of the water surface is covered by broken ice (Case No. 2, 4, and 6), the difference between the speed of oil spread in different average flow velocity is almost the same as those in flow with 10% ice concentration.

The areal extent of the oil-contaminated zone is another critical dimension to spreading (Vankatesh et al., 1990). For analysis of this dimension, Fig. 4.6 and Fig. 4.7 compare how spilled oil tends to transport in different directions and how much the maximum oil volume fraction varies by changing the average flow velocity at the inlet. The maximum oil volume fraction in all directions will be increased more than two times when the average flow velocity changed from 0.1 m/s to 0.3 m/s no matter how many percentages of the water surface is covered by the broken ice. Interestingly, when the average flow velocity increase from 0.3 m/s to 0.5 m/s for the flow ith 10% ice concentration, the maximum oil volume fraction in all directions will be reduced slightly, but for the flow with the higher ice concentration (30%), this amount did not change. Although the extent of spreading the oil in x-direction was significantly affected by increasing the average flow velocity in flows with different ice concentration (10% and 30%), the extent of spreading in z-direction will be changed increasingly, specifically in flow with higher ice concentration, by changing the average flow velocity. The higher the average flow velocity, the oil spreads more in the z-direction.

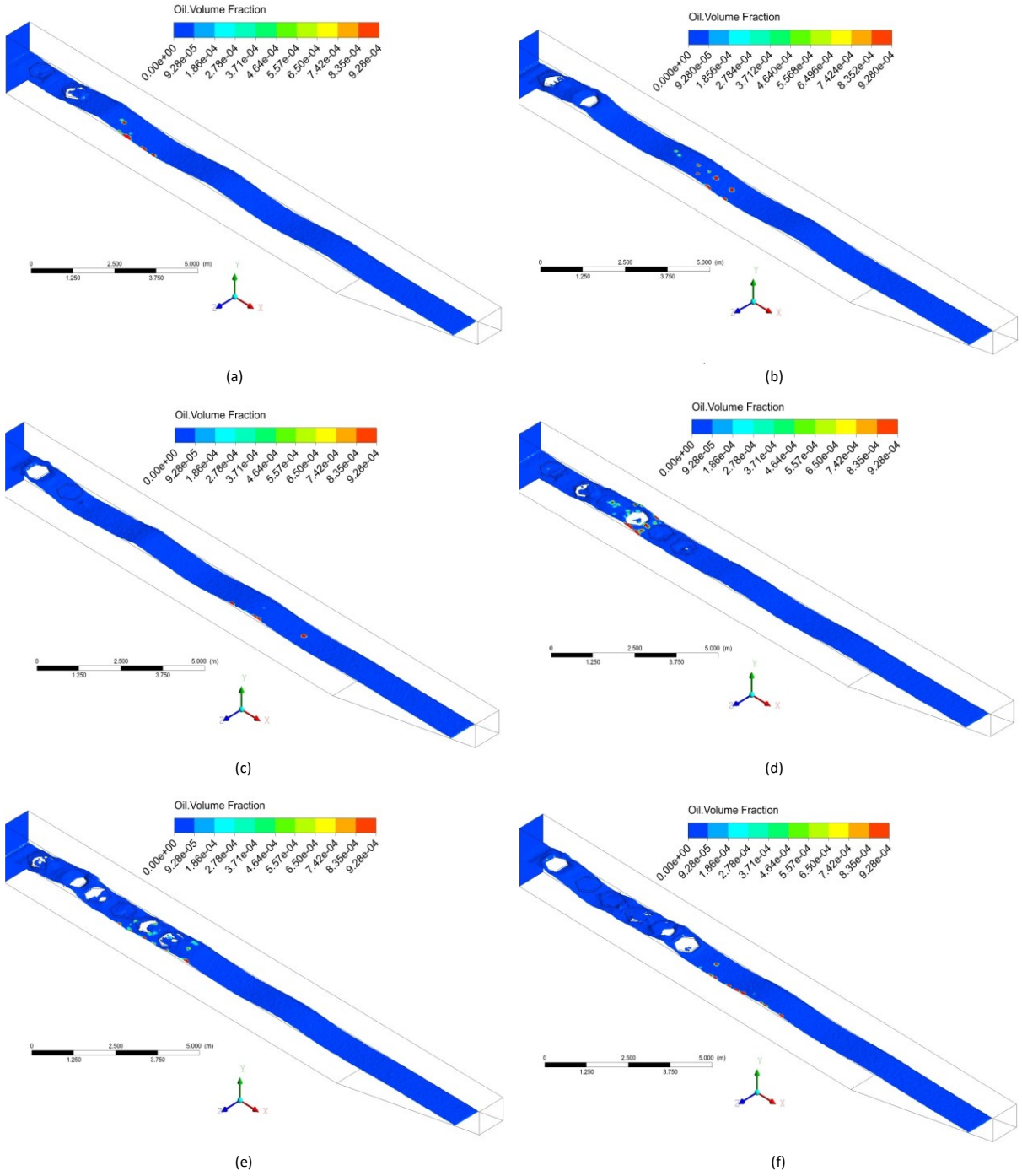

Fig. 4.6. Contour of oil volume fraction at the water surface for Sable Island Condensate oil at t = 18 s with the wave number of one: (a) the ice concentration is 10% and u = 0.1 m/s; (b) the ice concentration is 10% and u = 0.3 m/s; (c) the ice concentration is 10% and u = 0.5 m/s; (d) the ice concentration is 30% and u = 0.1 m/s; (e) the ice concentration is 30% and u = 0.3 m/s; (f) the ice concentration is 30% and u = 0.5 m/s.

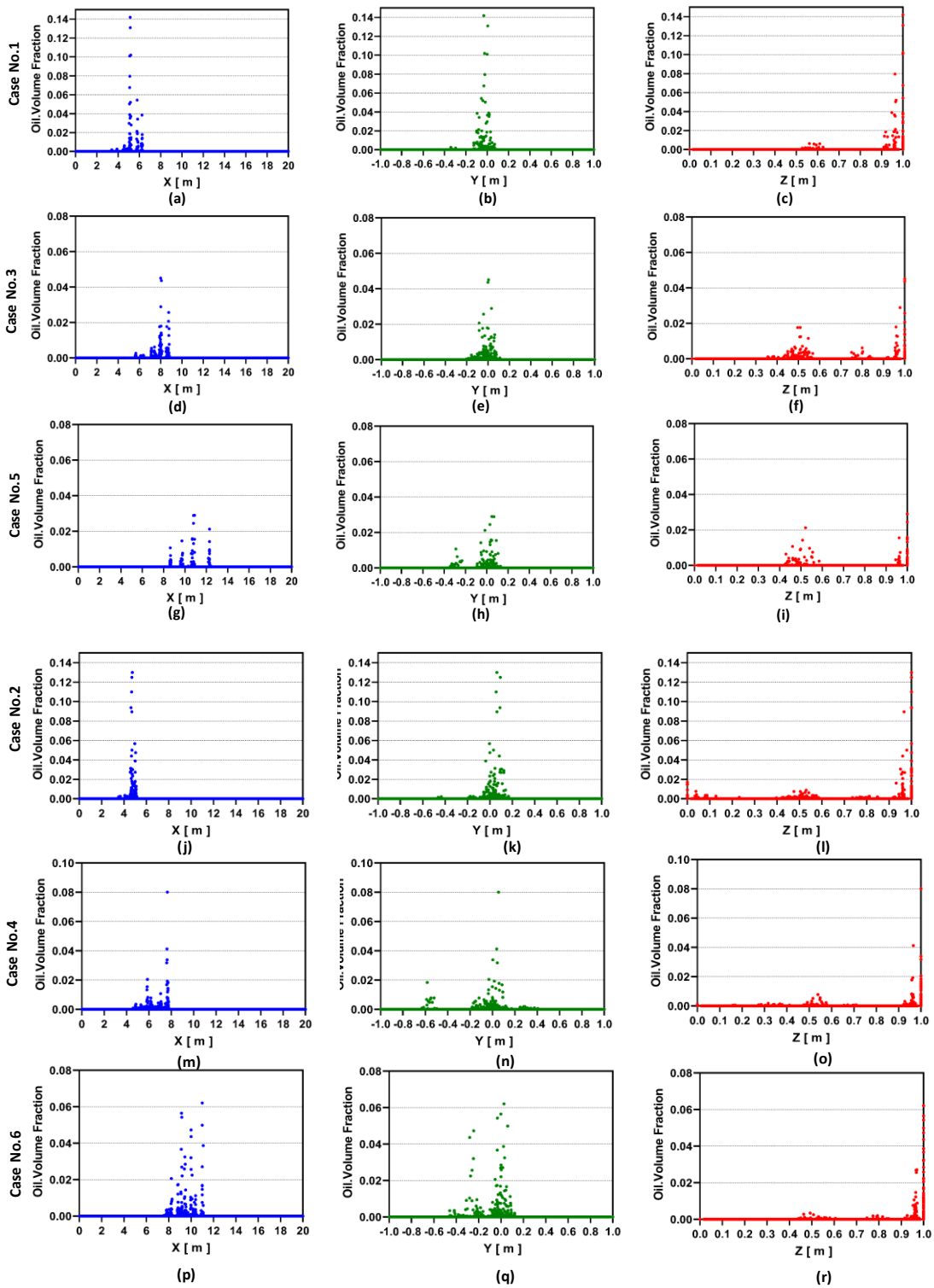

Fig. 4.7. Oil volume fraction in x, y, and z-directions for different Case Numbers at t= 18 s, and constant wave number.

The range of oil migration in the y-direction, when the ice concentration is 10%, changes slowly with the average flow velocity. By increasing the average flow velocity, as shown in Fig 4.7b, 4.7e, and Fig.4.7h. The oil migration is at the initial water surface (y = 0 m) mostly, and increasing the flow velocity makes the spilled oil more likely to move toward the seafloor. These changes in the level of oil migration with average flow velocity are rapid when the ice covers 30% of the water surface area (Fig.4.7k, Fig.4.7n, and Fig.4.7q). Consequently, decreasing the average flow velocity makes the spilled oil transports less diluted in y-directions, mostly at the water surface.

4.3.4. Effect of Wave on Nearshore Oil Behaviors

The diffusion of spilled oil is a complex natural happening that combines factors such as the waves. The waves are particularly crucial in predicting the range of oil diffusion, and if they are appropriately considered, the range of oil diffusion can be predicted precisely (Korea Coast Guard (KCG), 2008). The wave is one of the significant ocean motion forms and could appear from sea surface to interior. To evaluate the effects of wave on spilled oil behavior, simulations were conducted by changing the wave number (k= 1 and 2), which leads to changing the wave frequency. The water temperature was 5 °C, the average flow velocity at the inlet is 0.1 m/s, and the ice concentration is 10%. Sable island condensate, Bunker C fuel oil, and Hibernia oil were considered for this section of the study. The effect of water on oil is more than buoyancy under the conditions of the sea wave. It means that by increasing the wave number, the oil will tend to move horizontally rather than vertically and laterally (Wei et al., 2013). Increasing the wave frequency by two times contributes to increasing the distance spilled oil migrates in the x-direction no matter what the spilled oil is (Fig. 4.8). This increase for Bunker C Fuel oil is the most; Hibernia and Sable Island condensate experience the same increase in the horizontal migration distance by changing the wave number from one to two. The maximum horizontal migration for Bunker C fuel oil, Sable Island, and Hibernia with k = 1 are 5.9 m, 6.2 m, and 6.2 m, respectively, while this distance for the flow condition with k = 2 is 10.2 m for all of the spilled oil. The similarity between the maximum oil distance in the x-direction for Hibernia and Sable Island is because their physical properties for these oils are almost the same at the water temperature of 5 °C. These results showed a good agreement with those of Anon (2011). By making a comparison between the results shown in Fig. 4.9 and Fig. 4.5 (Case No.1, Case No.6, Case No.8, and Case No.10), it can be pointed out that the

presence of ice damps the action of waves slightly. It means by increasing the ice concentration from 10% to 30%, the effect of wave on oil spreading would be reduced. The results agree to some points with the works done by Anon (1987) and Singsaas et al. (1994). They stated that in ice-covered waters, dispersion is not dominant, and ice-covered waters tend to damp the effects of waves. It can be found that although the wave frequency plays a crucial role in oil volume fraction, fate, and transport of spilled oil in ice-covered water, damping effects of the wave due to the presence of ice makes this factor less important than the impact of that in the ice-free water.

Moreover, Fig. 4.9 compares the effect of wave frequency on the oil volume fraction and spilled oil movement in y and z-direction for different oils. An increase of wave frequency makes spill oil moves more diluted in y and z-direction. When the wave number was changed from one to two, the maximum oil volume fraction was reduced by 50% for Bunker C fuel oil (from 0.09 to 0.042) and almost by 75% for Sable Island Condesnate and Hibernia (from 0.14 to 0.05). Also, the extent of oil movement in y-direction increased by two times for all of the oils, which means spilled oils are more likely to move toward the seafloor. Regarding the effect of wave frequency on the extend of oil spreading in the z-direction, it can be found that in the flow condition with a lower wave number (k =1), the spilled oil spreads less in the z-direction in different spilled oils. The maximum oil volume fraction in the flow with a lower wave number is much more than the flow condition with the higher wave number (k=2), regardless of the oil properties.

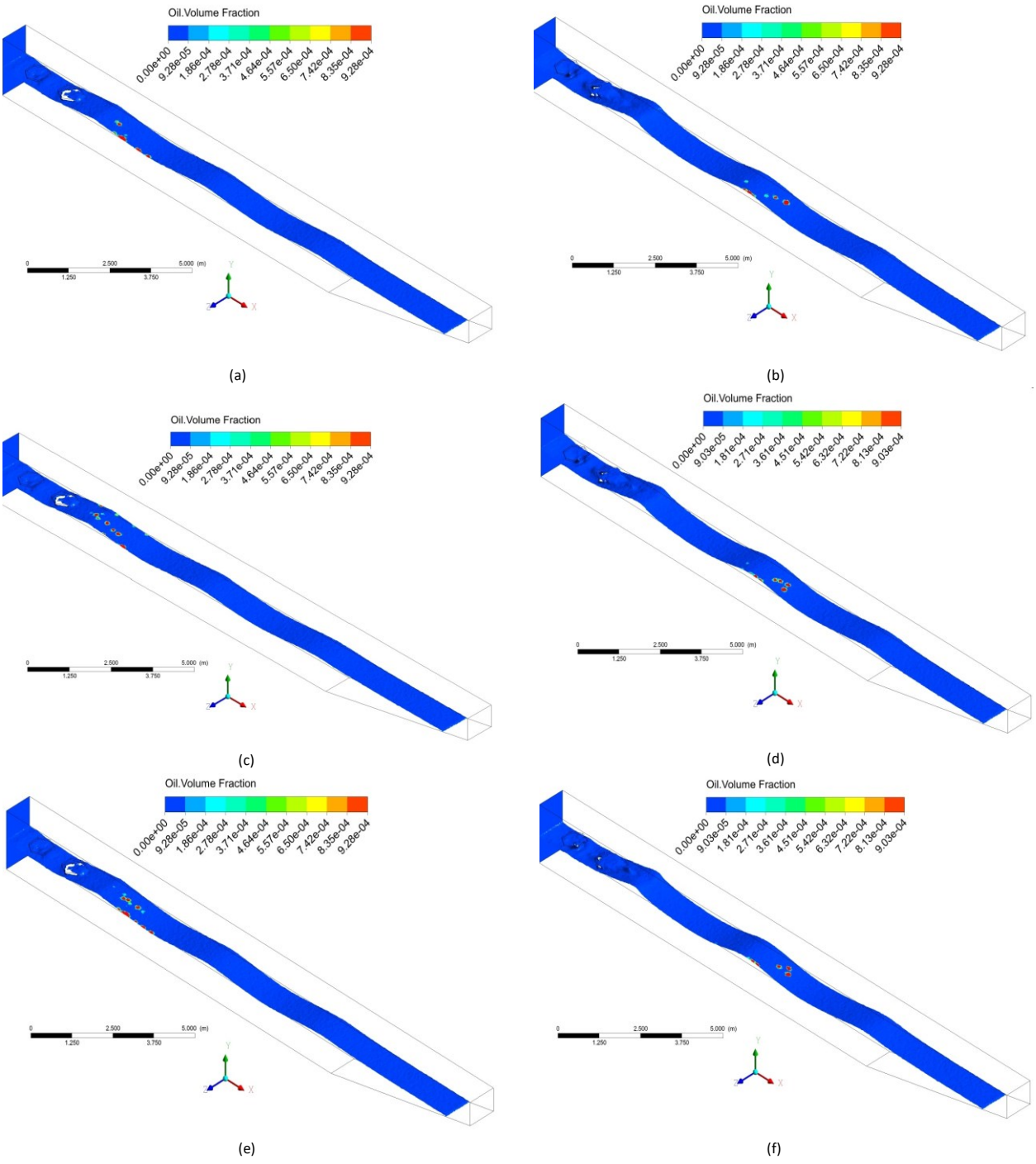

Fig. 4.8. Contour of oil volume fraction at the water surface for different oils at t = 18 s in flow with 10% ice concentration and u = 0.1 m/s: (a) the spilled oil is Sable Island Condensate and k = 1; (b) the spilled oil is Sable Island Condensate and k = 2; (c) the spilled oil is Bunker C fuel oil and k = 1; (d) the spilled oil is Bunker C fuel oil and k = 2; (e) the spilled oil is Hibernia and k = 1; (f) the spilled oil is Hibernia and k = 2.

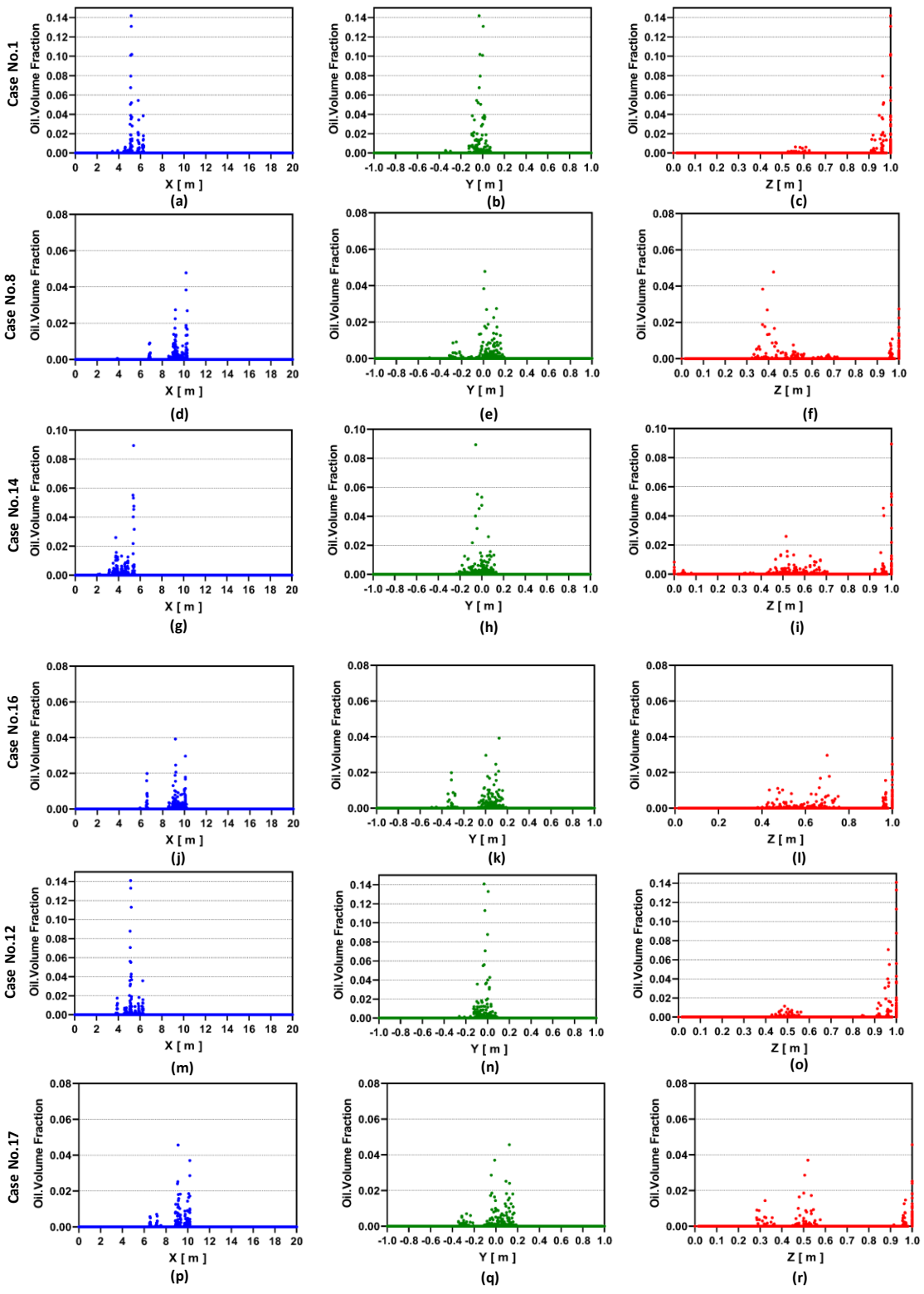

Fig. 4.9. Oil volume fraction in x, y, and z-directions for the flow with different wave frequency at t= 18 s, and constant average flow speed.

4.3.5. Effect of Oil Properties on Nearshore Oil Behaviors

The oil properties may range to a considerable extent (Badiozamani et al., 2019; Pi et al., 2017). Fate and transport of spilled oil are affected by their chemical and physical properties (Buist et al., 2013). Density, viscosity, and interfacial tension are important oil properties for spreading, emulsification, and dispersion (Fingas, 2015). In this section, to study the effect of oil properties on the fate and transport of oil and oil volume fraction, simulations were conducted (10% of the water surface is covered by ice and k = 1) for two average flow velocities (u= 0.1 m/s and 0.3 m/s) by changing the oil type, which led to changing oil density, oil dynamic viscosity and interfacial surface tension between oil and seawater while leaving other parameters the same. Three different oil, including Bunker C Fuel oil, Hibernia, and Sable Island Condensate, were taken into account for the analysis. Bunker C Fuel oil is a heavy oil (ρ = 976 g/mL at T = 5 °C), which its dynamic viscosity is extremely higher than the chosen oil. Hibernia is a light oil (ρ = 841 g/mL at T = 5 °C), which its interfacial surface tension with the seawater is relatively lower than the other mentioned oils, and Sable Island Condensate is light oil (ρ = 839 g/mL at T = 5 °C). The oil properties were based on information provided by Environment and Climate Change Canada (Environment and Climate Change Canada, Oil Properties Database, 2001).

Fig. 4.10 and Fig .4.11 illustrate the process of oil migration in the horizontal, vertical, and lateral directions for different oils, and also, the change of oil volume fraction after 18 seconds flow has been shown in Fig. 4.11. It can be seen that the horizontal migration of spilled oils has not shown a meaningful difference when the average flow speed is 0.1 m/s, spilled oil spread between 4 m to 6 m distance of the inlet area. Bunker C oil's maximum oil volume fraction is lower than those of Sable island condensate and Hibernia, 0.09 and 0.14, respectively. The results for Sable Island and Hibernia, whose surface tensions are almost the same, could be acceptable because apart from highly viscous oils, the oil will generally spread because of its unique surface tension (Buist et al., 2013). Besides that, the results are similar to those reported by Zhu et al. (2017), in which only different oil densities were considered for horizontal-migration evaluation, and also, in the mentioned study, the presence of ice was not being taken into account. When the average flow speed at the inlet is 0.3 m/s, Bunker C fuel moved relatively slowest, and it could be because of its too high density, although its high dynamic viscosity should help it move with the water current. Regarding the maximum oil volume fraction in the flow with u= 0.3 m/s, it could

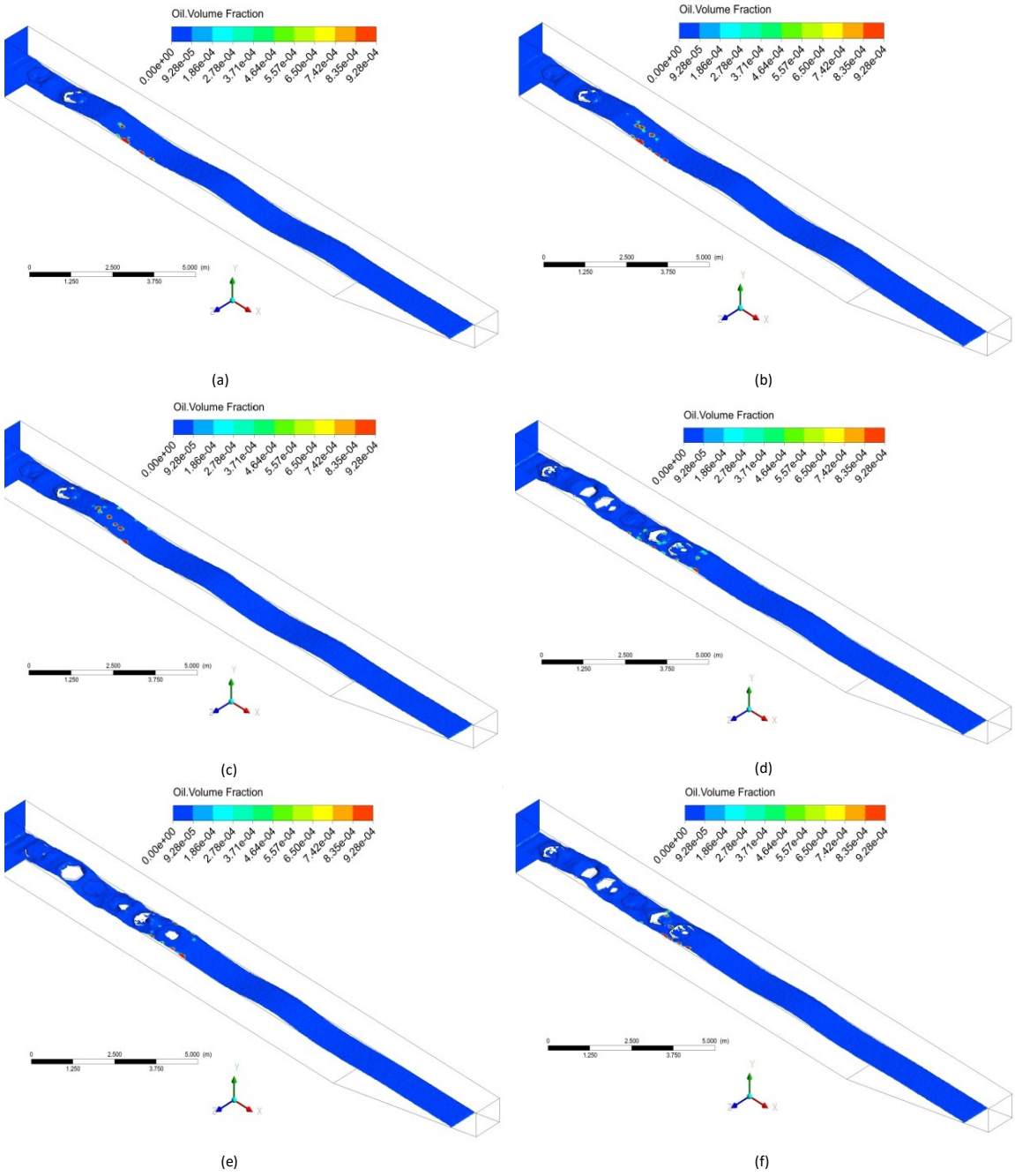

Fig. 4.10. Contour of oil volume fraction at the water surface for different oils at t = 18 s in flow with 10% ice concentration: (a) the spilled oil is Sable Island Condensate and u = 0.1 m/s; (b) the spilled oil is Hibernia and u = 0.1 m/s; (c) the spilled oil is Bunker C fuel oil and u = 0.1 m/s; (d) the spilled oil is Sable Island Condensate and u = 0.3 m/s; (e) the spilled oil is Hibernia and u = 0.3 m/s; (f) the spilled oil is Bunker C fuel oil and u = 0.3 m/s.

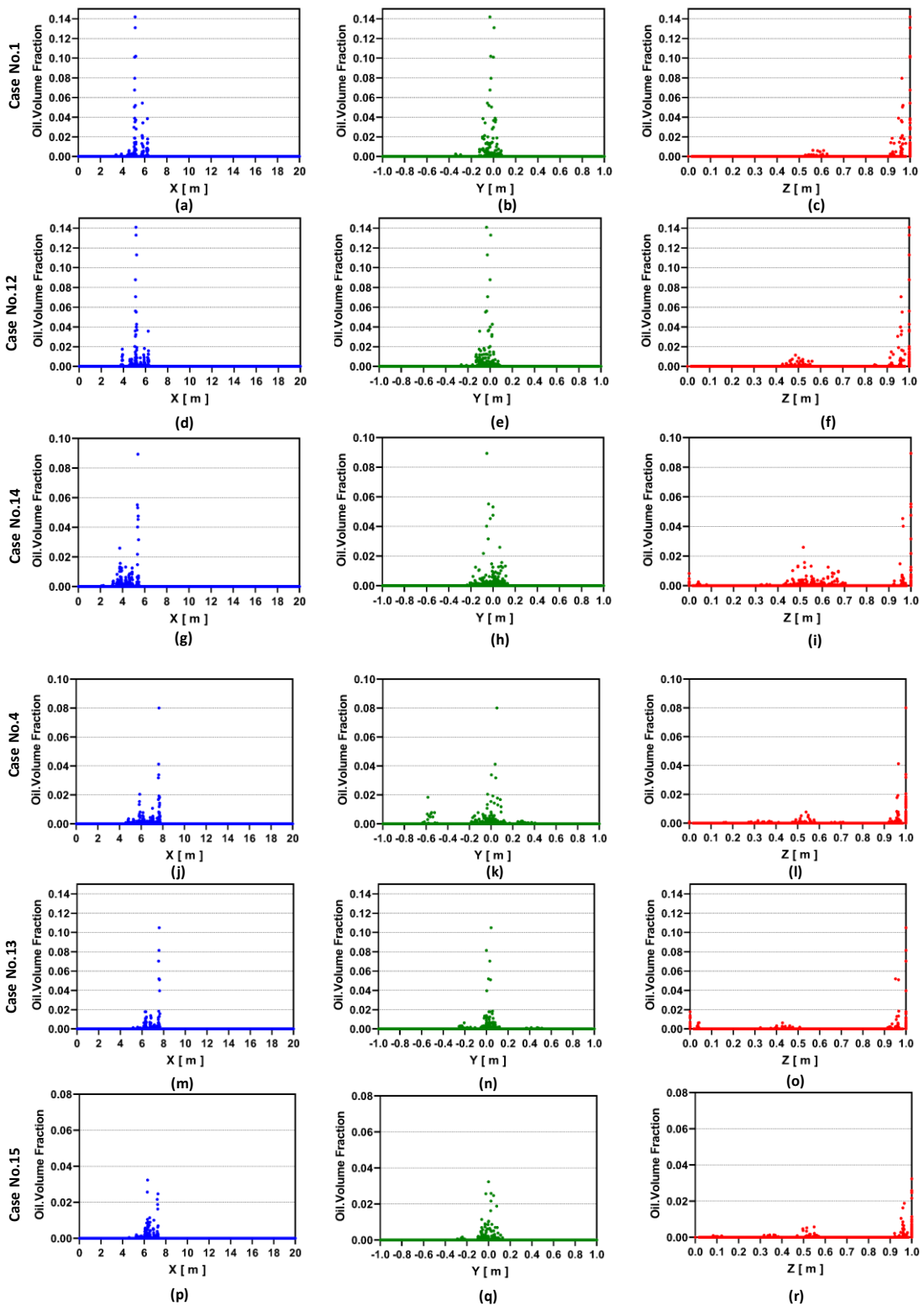

Fig. 4.11. Oil volume fraction in x, y, and z-directions for the flow with different oil types at t= 18 s, and constant ice concentration.

be found that Sable Island moves in the x-direction with lower oil volume fraction. Whose density is the lowest, and its interfacial surface tension with water is relatively larger than those of Hibernia and lower than Bunker C oil.

Based on Fig.4.11, Bunker C fuel oil in y-direction moves more diluted than the other ones in both flow conditions, u = 0.1 m/s and 0.3 m/s, because its maximum oil volume fraction is lower than the ones, and its extent of spreading in vertical direction larger than those of Hibernia and Sable island oils. It could be explained by the higher density, interfacial surface tension, and dynamic viscosity of Bunker C in comparison to those of other oils. The condition for the migration in the z-direction is ultimately looked like the spreading of spilled oils in the y-direction.

4.4. Summary

In this study, oil behaviors for the ice-covered water in the nearshore area under the different ice concentrations, wave conditions, average flow velocities, and oil properties were investigated to understand the fate and transport of oil, which is a key in developing emergency spill response models. The problem is simulated by a fluid dynamics model (VOF model) coupled with the general equations of the rigid body motion (Six Degree of Freedom or 6-DOF) with the help of Ansys Fluent. It was found that the presence of ice retards the spreading of spilled oil because the ice can create natural barriers to oil movement; the higher the ice concentration, the slower spilled oil migrates in all directions, and the maximum oil volume fraction will be increased by about two times by increasing the ice coverage on the water surface area from 10% to 30% under the same flow condition no matter how much the wave number is. Consequently, decreasing the ice concentration makes the spilled oil transport more diluted.

The wave frequency, the averaged flow velocity, and oil properties would affect the oil spread extent and the oil volume fraction. The higher the averaged flow velocity, the faster the oil movement in all directions, and decreasing the average flow velocity makes the spilled oil transports less diluted in y-directions, mostly at the water surface. Increasing the wave frequency by two times, leads to increasing the distance spilled oil migrates in the x-direction, regardless of what the oil properties are. Also, the dumping effect of the wave due to the presence of ice makes the impact of this factor less important than those in the open water. Finally, it was found that the horizontal migration of different spilled oils have not shown a meaningful difference when the

average flow speed is 0.1 m/s, but when the average flow speed at the inlet is 0.3 m/s, Bunker C fuel moved relatively slowest, and it could be because of its too high density. Also, Bunker C fuel oil in y and z-direction moves more diluted than the other ones in both flow conditions. The effects of some other environmental factors, like encapsulation and evaporation, can be further investigated in future studies.

CHAPTER 5. CONCLUSIONS

5.1. Conclusions

Understanding the nearshore oil behaviors is essential for assessing oil spill risk for shorelines, and the fate and behavior of the spilled oil will also impact spill response effectiveness. Previous research mainly focused on either the computational simulation of the regular waves in deep-water or the CFD simulation of oil leakage from submarine pipelines. Due to the lack of detailed computational studies for the fate and transport of spilled oil under the action wave and other environmental factors for the open water and ice-covered water near the shore area, the 3D simulations of wave propagation in shallow water conducted for open water and ice-covered water to investigate the behaviors of spilled oil in the nearshore area under different boundary conditions.

In the first part of the current study, it was focused on the numerical simulation of the nearshore oil behaviors based on computational fluid dynamics. Based on the Navier-Stokes momentum equations for an incompressible viscous fluid and VOF method, a 3D numerical model of three-phase transient flow was developed. Effects of different average flow velocities at the inlet (u= 0.1 m/s and 1 m/s), different wave frequency (k=1 and 2) in two different water temperatures (15 and 5 °C) for Bunker Fuel oil, Hebron oil, Hibernia oil on fate and transport of spilled oil nearshore area were investigated. Also, the results compared with those of previous computational studies.

In the next part, a fluid dynamics model (VOF model) coupled with the general equations of the rigid body motion (Six Degree of Freedom or 6-DOF) simulated. The wave propagation in the shallow water with different broken ice coverage (10%, 30%, and 50%) to investigate the behaviors of spilled oil in the nearshore area under different wave frequency (k= 1 and 2), different averaged flow velocity (u= 0.1 m/s and 0.3 m/s) and for different oils (Sable Island Condensate, Hibernia, and Bunker C fuel oil). The results compared with previous studies and, in some parts, showed a good agreement.

5.2. Research Contributions

In this study, the fate and transport of spilled oils in nearshore areas under different boundary conditions have been investigated. The following findings have been achieved.

- In the ice-free waters, the wave frequency and averaged water velocity are the most effective factors influencing the fate and transport of the spilled oil in nearshore area.
- In the ice-covered waters, the percentages of water surface area covered by the broken ice, the wave frequency, and the averaged flow velocity are main factors influencing the spilled oil behavior.
- The wave frequency plays a crucial role in oil volume fraction, fate, and transport of spilled oil in ice-covered water. Damping effects of the wave due to the presence of ice makes this factor less important than its impact in the ice-free water.
- The main difference between the different oil types is viscosity. The increased oil viscosity may cause decreased spreading rates. However, the effects of waves, ice concentration and water currents are more significant.

5.3. Recommendations for Future Research

The present work investigated the fate and transport spilled oil nearshore area by using the VOF model. Research focusing on the following areas can be further conducted in the future.

- This 3D model has not considered other environmental factors like evaporation and encapsulation. Further simulations should consider such processes. Multiphase evaporation models with heterogeneous heat and mass transfer could be considered for evaporation.
- Simulations of a two-phase flow model (water and air), with a particle tracking system to simulate individual oil droplets in nearshore area, can be conducted under different boundary conditions.
- Other physics in CFD model, like particulate, can be considered by using agglomeration kernels in the population balance model and level set plus VOF.
- The dissolution process, mixing or reactions can be further considered to better predict the oil behavior.

- It is worth investigating the crashing of the waves on the beach by considering the violence of the breaker and considering its impact on oil volume fraction.
- It is worth investigating the oil behavior in nearshore area coupled and considering the impacts of underground flow on the shoreline.

REFERENCES

Abascal, A., Castanedo, S., Medina, R., Liste, M., 2010. Analysis of the reliability of a statistical oil spill response model. *Marine Pollution Bulletin*. 60 (11), 2099–2110.

Afenyo, M., Veitch, B., Khan, F., 2016. A state-of-the-art review of fate and transport of oil spills in open and. *Ocean Engineering*. 119, 233–248.

Agrawal, M., Dakshinamoorthy, D., ANSYS Inc, 2011. Computational analysis of oil spill in shallow water due to wave and tidal motion, Offshore Technology Conference, Houston, Texas, USA DOI: 10.4043/21949-MS.

An, C., Huang, G., Yao, Y., Zhao, S., 2017. Emerging usage of electrocoagulation technology for oil removal from water: A review . *Science of The Total Environment (Elsevier)*. 579, 537-556 .

Anon., 1987. Prepared for S.L. Ross Environmental Research Limited (SL Ross) and DF Dickins Associates Ltd. (DF Dickins). Field research spills to investigate the physical and chemical fate of oil in pack ice. Environmental Studies Revolving Funds, Report No. 062, Ottawa.

Anon, 2003. Oil in the Sea III: Inputs, fates, and effects. National Research Council, Division on Earth and Life Studies, Transportation Research Board, Marine Board, Ocean Studies Board, Prepared for National Research Council, Washington D.C, 2003.

Anon., 2011. Prepared for International Tanker Owners Pollution Federation Limited (ITOPF). Fate of marine oil spills. *Technical information paper*.

Badiozamani, M.M., Ben-Awuah, E., Askari-Nasab, H., 2019. Mixed integer linear programming for oil sands production planning and tailings management. *Journal of Environmental Informatics*. 33(2), 96-104.

Beegle-Krause, C.J., Simmons, H., McPhee, M., Daae, R.L., Reed, M., 2013. Fate of Dispersed Oil Under Ice Final Report 1.4 Literature Review, Arctic Oil Spill Response Technology Joint Industry Programme (JIP) p. 48.

Bobra, A.M., Fingas, M.F., 1986. The behaviour and fate of Arctic oil spills. *Water Science &Technology.* 18, 13–23.

Brackbill, J.U., Kothe, D.B., Zemach, C., 1992. A continuum method for modeling surface tension. *Journal of Computational Physics*. 100 (2), 335-354.

Brandvik, P., Faksness, L., 2009. Weathering processes in the Arctic oil spills: Mesoscale experiments with different ice conditions. *Cold Regions Science and Technology*. 55, 160–166.

Brandvik, P.J., Sørheim, K.R, Reed, M., 2006. Short state-of-the-art report on oil spills in ice-infested waters (final). SINTEF A06148.

Boufadel, M.C, Cui, F., Katz, J., Nedwed, T., Lee, K., 2018. On the transport and modeling of dispersed oil under ice, *Marine Pollution Bulletin*. 135, 569–580.

Buist, I.A., Potter, S.G., Trudel, B.K., Shelnutt, S.R., Walker, A.H., Scholz, D.K., Brandvik, P.J., Fritt-Rasmussen., Allen, A.A., Smith, P., 2013. In situ burning in ice affected waters: State of Knowledge Report. Final report 7.1.1. Report from Joint Industry Program to present status of regulations related to in situ burning in Arctic and sub-Arctic countries.

Camp, J.S., LeBoeuf, E.J., Abkowitz, M.D., 2010. Application of an enhanced spill management information system to inland waterways. *Journal of Hazardous Material*. 175, 583–592.

Cao, Y., Zhang, B., Zhu, Z., Song, X., Cai, Q., Chen, B., Dong, G., Ye, X., 2020. Microbial eco-physiological strategies for salinity-mediated crude oil biodegradation. *Science of The Total Environment*, 138723.

Castanedo, S., Medina, R., Losada, I.J., Vidal, C., Méndez, F.J., Osorio, A., Juanes, J.A., Puente,A., 2006. The prestige oil spill in Cantabria (Bay of Biscay). Part I: operational forecasting. *Coastal Research*, 1474-1489.

Chang, S. E., J. Stone, K. Demes, and M. Piscitelli. 2014. Consequences of oil spills: a review and framework for informing planning. Ecology and Society 19(2): 26. http://dx.doi.org/10.5751/ES-06406-190226

Chao, X.B., Shankar, N.J., Cheong, H.F., 2001. Two- and three dimensional oil spill model for coastal waters, *Ocean Engineering*. 28 (12), 1557–1573.

Chen, Z.K., An, C., Boufadel, M., Owens, E., Chen, Z., Lee, K., Cao, Y., Cai, M., 2020. Use of surface-washing agents for the treatment of oiled shorelines: Research advancements, technical applications and future challenges. *Chemical Engineering Journal.* 391, 123565.

Chen, Z.K., An, C., Yin, J., Owens, E., Lee, K., Zhang, K., Tian, X., 2021. Exploring the use of cellulose nanocrystal as surface-washing agent for oiled shoreline cleanup. *Journal of Hazardous Materials*. 402, 123464.

Clauss, G.F., Schmittner, C.E., Stuck, R, 2005. Numerical wave tank - simulation of extremewaves for the investigation of structural responses. *In: Proceedings, 24th International Conference on Offshore Mechanics and Arctic Engineering.* Halkidiki, Greece.

Coastal engineering research center 1984, U.S Army Coastal Engineering Research Center.

Cui, F., Zhao, L., Daskiran, C., King, T., Lee, K., Katz, J., Boufadel, M.C., 2020. Modeling oil dispersion under breaking waves. Part II: Coupling Lagrangian particle tracking with population balance model, *Environmental Fluid Mechanics*, DOI 10.1007/s10652-020-09759-1.

Dean, R.G., Dalrymple, R.A, 1984. Water Wave Mechanics for Engineers and Scientists. New Jersey: Prentice Hall, Englewood Cliffs.

Delvigne, G., Sweeney, C.E., 1988. Natural dispersion of oil. *Oil and Chemical Pollution*. 4, 281–310.

Devolder, B., Troch, P., Rauwoens, P., 2018. Performance of a buoyancy modified k-ω and k-ω SST turbulence model for simulating wave breaking under regular waves using OpenFOAM. *Coastal engineering. 138, 49-65.*

Drozdowski, D., Nudds, S., Hannah, C.G., Niu, H., Peterson, I., Perrie, W., 2011. Review of oil spill trajectory modelling in the presence of ice, Canadian Technical Report of Hydrographic and Ocean Sciences. Fisheries and Ocean, Canada, p. 274.

Elangovan, M., 2011. Simulation of irregular waves by CFD. *International Journal of Mechanical, Aerospace, Industrial, Mechatronic and Manufacturing Engineering*. 5 (7), 1379 1383.

Elliott, A. J. 1986. Shear diffusion and the spread of oil in the surface layers of the North Sea. Deutsche Hydrographische Zeitschrift 39:113-137.

Elshorbagy, W. E., 2006. Hydrodynamic characterization and modelling of the Persian Gulf. *Journal of Waterway, Port, Coastal and Ocean Engineering.* 132 (47), 47–56.

Elshorbagy, W. E., 2008. Risk assessment maps of oil spill for major desalination plants in the United Arab Emirates. *Desalination*. 228,200–216.

Environment and Climate Change Canada, Oil Properties Database. 2001. Retrieved from http://www.etc-cte.ec.gc.ca/databases/oilproperties.

Evers, K.U., Jensen, H.V., Resby, J.M., Ramstad, S., Singsaas, I., Dieckmann, G., and Gerdes, B., 2004. State-of-the-Art Report on Oil Weathering and on Effectiveness of Response Alternatives. Report of ARCOP Work package 4 Environmental Protection and Management System for the Arctic, GROWTH Project GRD2- 2000-30112 "ARCOP", available as ARCOP WP4 Report 4.2.1.1(a), 2004, ⟨http:// www.arcop.fi⟩., retrieved on 23-01-2015.

Faghihifard, M., Badri, M.A., 2016. Simulation of oil pollution in the Persian Gulf near Assaluyeh oil terminal. *Marine Pollution Bulletin*, 143–149.

Faksness, L.G., Brandvik, P.J., Daae, R.L., Leirvik, F., Børseth, J.F., 2011. Large-scale oil-in-ice experiment in the Barents Sea: monitoring of oil in water and Metocean interactions. *Marine Pollution Bulletin*. 62 (5), 976–984.

Fay, J.A. 1969. The spread of oil slicks on a calm sea–oil on the sea. Plenum, New York. Pp 53-64.

Fingas, M., 2012. *The Basics of Oil Spill Cleanup* (Third Edition ed.).

Fingas, M. (Ed.), 2015. Handbook of oil Spill Science and Technology. John Wiley and Sons, New Jersey, ISBN 978-0-470-45551-7.

Fingas, M.F., Hollebone, B.P., 2003. Review of behaviour of oil in freezing environments. Marine Pollution Bulletin. 47 (9–12), 333–340.

Finnegan, W., Goggins, J., 2012. Numerical simulation of linear water waves and wave structure interaction. *Ocean Engineering. 43*, 23-31.

French-McCay, D.P., 2004. Oil spill impact modeling: development and validation. *Environmental Toxicology and Chemistry. 23*, 2441–2456.

French McCay, D.P., Jayko, K., Li, Z., Horn, M., Kim, Y., Isaji, T., Crowley, D., Spaulding, M., Decker, L., Turner, C., Zamorski, S., Fontenault, J., Shmookler, R., Rowe, J.J., 2015. Technical Reports for Deepwater Horizon Water Column Injury Assessment – WC_TR14: Modeling Oil Fate and Exposure Concentrations in the Deepwater Plume and Cone of Rising Oil Resulting from the Deepwater Horizon Oil Spill. DWH NRDA Water Column Technical Working Group Report. Prepared for National Oceanic and Atmospheric Administration by RPS ASA, South Kingstown, RI, USA. September 29, 2015. Administrative Record no. DWH-AR0285776.pdf. https://www.doi.gov/deepwaterhorizon/adminrecord.

French-McCay, D.P., Tajalli-Bakhsh, T., Jayko, K., Spaulding, M.L., Li, Z., 2017. Validation of oil spill transport and fate modeling in Arctic ice. *Arctic Science*. 4 (0), 71–97.

Galt, J. A. and R. Overstreet, 2011. Development of spreading algorithms for the response options calculator (ROC), by Genwest Systems, Inc., (Genwest Technical Publication 11-003).

Gao, F., Zhao L, Boufadel, M., King T., Robinson B., Conmy, R., Miller, R. 2017. Hydrodynamics of oil jets without and with dispersant: experimental and numerical characterization. *Applied Ocean Research. 68,* 77–90.

Geng, X., Boufadel, M., Rajaram, H., Cui, F., Lee, K., An, C., 2020. numerical study of solute transport in heterogeneous beach aquifers subjected to tides. *Water Resources Research (American Geophysical Union)*, 56(3).

Gjøsteen, J.K. Ø., Løset, S., 2004. Laboratory experiments on oil spreading in broken ice, Cold Regions Science and Technology. 38, 103-116.

Guide, ANSYS Fluent Theory, 2013.

Guo, W.J., Wang, Y.X., Xie, M.X., Cui, Y.J., 2009. Modeling oil spill trajectory in coastal watersbased on fractional Brownian motion. *Marine Pollution Bulleetin. 58*, 1339–1346.

Hānninen, S., Sassi, J., 2010. Acute Oil Spills in Arctic Waters-Oil Combating in Ice, VTT Research Report VTT-R-03638-09.

Han, Z., Liu, Z., Shi, H., 2018. Numerical study on overtopping performance of a multilevel breakwater for wave energy conversion. *Ocean Engineering*. 150, 94–101.

Havn, J., 2011. *Wave Loads on Underwater Protection Covers.* Trondheim, Norway: Master thesis in Ocean Engineering. Department of Marine Technology, Norwegian University of Science and Technology (NTU).

Hebron., 2001. Environment and Climate Change Canada, Oil Properties Database. Retrieved from http://www.etc-cte.ec.gc.ca/databases/oilproperties.

Hester, M. W., Willis, J. M., Rouhani, S., Steinhoff, M. A., Baker, M. C., 2016. Impacts of the Deepwater Horizon oil spill on the salt marsh vegetation of Louisiana. *Environmental Pollution*. 216, 361-370.

Hibernia., 2001. Environment and Climate Change Canada, Oil Properties Database. Retrieved from http://www.etc-cte.ec.gc.ca/databases/oilproperties.

Hongjun, Z., 2017. An experimental investigation of underwater spread of oil spill in a shear flow. *Marine Pollution Bulletin. 116* , 156–166.

Hotte, N., Sumaila, U.R., 2012. A Research Report from the Fisheries Centre at UBC with support from WWF-Canada 45 pages © Fisheries Centre, University of British Columbia, 2012.

Hoult, D.P., 1972. Oil spreading on the sea. *Annual Review of Fluid Mechanic*. 341–367.

Izumiyama, K., Konno, A., Sakai, S., 2002. Experimental Study on Spreading of Oil under Ice Covers, International Offshore and Polar Engineering Conference, Kitakyushu, Japan.

Johansen. O, 2000. Deep blow-a Lagrangian plume model for deep water blowouts. *Spill Scienc & Technology Bulletin*. 6 (2), 103–111.

Johansen, O., 2002. Estimates of droplet size from subsea oil and gas leaks or blowouts. SINTEF document, Norway.

Johansen, Ø., Brandvik, P.J., Farooq, U., 2013. Droplet breakup in subsea oil releases– part 2: predictions of droplet size distributions with and without injection of chemical dispersants. *Marine Pollution Bulletin*. 73 (1), 327–335.

Johansson, A. M., Eriksson, L.E.B., HassellÖv, I., Landquist, H., Berg, A., and Carvajal, G., 2013. Remote sensing for risk analysis of oil spills in the arctic ocean. Proceedings of the ESA Living Planet Symposium 2013, 9-13 September 2013.

Kh, M.Z.K., Mazaheri, S., Mazyak, A.R., 2017. Wave generation in a numerical wave tank.

International Journal of Coastal & Offshore Engineering. 5, 33–43.

Korea Coast Guard (KCG). 2008, Korea Coast Guard 2008 White Paper; Korea Coast Guard: Seoul, Korea.

Kundu, S., Ghoshal, K., 2019. An entropy based model for velocity-dip-position. *Journal of Environmental Informatics*. 33(2). 113-128.

Lal, A., Elangovan, M., 2008. CFD simulation and validation of flap type wave-maker. *International Journal of. Mathematical, Computational, Physical, Electrical. and Computer Engineering.* 2 (10), 708–714.

Lee, K.(chair), Boufadel, M., Chen, B., Foght, J., Hodson, P., Swanson, S., Venosa, A., 2015. Expert Panel Report on the Behaviour and Environmental Impacts of Crude Oil Released into Aqueous Environments. Royal Society of Canada, Ottawa, ON. ISBN: 978-1-928140-02-3.

Lee, M., Jung, J., 2015. Pollution risk of assessment of oil spill accidents in Garorim Bay ofKorea. *Maine. Pollution Bulletin. 100*, 297–303.

Lehr, W.J., Wesley, D., Simecek-Beatty, D., Jones, R., Kachook, G., Lankford, J., 2000. Algorithm and interface modifications of the NOAA oil spill behavior model. Proceedings of the 23rd Arctic and Marine Oil Spill Program (AMOP) Technical Seminar, Vancouver, BC. Environmental Protection Service, Environment Canada, pp. 525–539.

Leibovich, S., 1983. The form and dynamics of Langmuir Circulations. *Annual Review of Fluid Mechanic*. 15, 391–427.

Leibovich, S., 1997. Surface, and near-surface motion of oil in the sea. Final Report. Contract 14-35-0001-30612. Mineral Management Service, Department of Interior.

Li, J., Li, S.S., 2020. Near-bed velocity and shear stress of open-channel flow over surface roughness. *Environmental Fluid Mechanics - Springer*. doi: DOI: 10.1007/s10652-019-09728-3.

Li, W., Liang, X., Lin, J., 2013. Mathematical model and computer simulation for oil spill in ice waters around island based on FLUENT, *Journal of Computers*, Vol. 8, No. 4.

Li, W., Pang, Y., Lin, J., Liang, X., 2013. Computational modeling of submarine oil spill with current and wave by FLUENT. *Research Journal of Applied Sciences, Engineering and Technology. 5(21)*, 5077-5082.

Li, X.H., Chen, G.M., Zhu, H.W., 2017. Modelling and assessment of accidental oil release from damaged subsea pipelines. *Marine Pollution Bulletin*. 123, 133–141.

Mackay, D., McAuliffe, C.D., 1988. Fate of hydrocarbons discharged at Sea. *Oil Chemical Pollution*. 5, 1–20.

Mackay, D., Shiu, W.Y., Hossain, K., Stiver, W., McCurdy, D., Peterson, S., 1982. Development and calibration of an oil spill behavior model. Report No. CG-D-27-83. U.S. Coast Guard, Research and Development Center, Groton, Connecticut, p. 83.

Maguire, A.E., 2011. *Hydrodynamics, Control and Numerical Modelling of Absorbing Wavemakers.* The University of Edinburgh.

Marques Machado, F.M., Gameiro Lopes, A.M., Ferreira, A.D., 2018. Numerical simulation of regular waves: Optimization of a numerical wave. *Ocean Engineering. 170*, 89–99tank.

McNutt, M., Camilli, R., Guthrie, G., Hsieh, P., Labson, V., Lehr, B., Maclay, D., Ratzel, A., Sogge, M., 2011. Assessment of flow rate estimates for the Deepwater Horizon/ Macondo Well oil spill. Washington, D.C.

MelakuCanu, D., Solidoro, C., Bandelj, V., Quattrocchi, G., Sorgente, R., Olita, A., Fazioli, L., Cucco, A., 2015. Assessment of oil slick hazard and risk at vulnerable coastal sites. *Marine Pollution Bulletin. 94*, 84–95.

Nagheeby, M., Kolahdooza, M., 2010. Numerical modeling of two-phase fluid flow and oilslick transport in estuarine water. *International Journal of Environvironmental Science & Technology. 7 (4)*, 771–784.

Ning, D.Z., Teng, B., 2007. Numerical simulation of fully nonlinear irregular wave tank in three dimension. *International Journal of Numerical Methods Fluid. 53*, 1847–1862.

Nissanka, I.D., Yapa, P.D., 2016. Calculation of oil droplet size distribution in an underwater oil well blowout. *Journal of Hydraulic Research*. 54 (3), 1–14.

Nixon, Z., Michel, J., 2015. Predictive modeling of subsurface shoreline oil encounter probability from the Exxon Valdez oil spill in Prince William sound Alaska. *Environvironmental Science & Technology. 49*, 4354–4361.

Ocean Studies Board and Marine Board, National Research Council, 2003. *Oil in the Sea III: Inputs, Fates, and Effects.* Washington: The National Academies Press.

Nyman, T. 2009. Evaluation of methods to estimate the consequence costs of an oil spill. SKEMA Seventh Framework Programme, Athens, Greece.

Pi, Y., Chen, B., Bao, M., Fan, F., Cai, Q., Ze, L., Zhang, B., 2017. Microbial degradation of four crude oil by biosurfactant producing strain Rhodococcus sp. *Bioresource technology*. 232, 263-269.

Reed, M., Daling, P., Brakstad, O., Singsaas, I., Faksness, L., Hetland, B., Ekrol, N., 2000. Oscar: a multi-component 3-dimensional oil spill contingency and response model. Proceedings of the Arctic and Marine Oil Spill Program (AMOP) Technical Seminar, Vancouver, CA, pp. 663–680.

Reed, M., Johansen, Brandvik, P.J., Daling, P., Lewis, A., Fiocco, R., Mackay, D., Prentki, R., 1999. Oil spill modeling towards the close of the 20th century: overview of the stateof the art. *Spill Science & Technology Bulletin. 5*, 3–16.

Romero, Isabel C., Toro-Farmer, G., Diercks, A.R., Schwing, P., Muller-Karger, F., Murawski, S., Hollander, D.J., 2017. Large-scale deposition of weathered oil in the Gulf of Mexico following a deep-water oil spill. *Environmental pollution*. 228, 179-189.

Sayol, J.M., Orfila, A., Simarro, G., Conti, D., Renault, L., Molcard, A., 2014. A Lagrangian model for tracking surface spills and SaR operations in the ocean, *Environmental Modelling and Software*. 52, 74–82.

Sebastiao, P., Soares, C.G., 1995. Modelling the fate of oil spills at sea. *Spill Science & Technology Bulletin. 2 (2/3)*, 121–132.

Shrestha, N. K., Wang, J., 2020. Water quality management of a cold climate region watershed in changing climate. *Journal of Environmental Informatics*. 35(1).

Silva, M.C., Vitola, M. de A., Pinto, W.T., Levi, C.A., 2010. Numerical simulation of monochromatic wave generated in laboratory: validation of a CFD code. *In: Atas do 23 Congresso Nacional de Transporte Aquaviário, Construção Naval E Offshore.* Riode Janeiro, Brasil.

Singsaas, I., Brandvik, P.J., Daling, P.S., Reed, M., Lewis., A., 1994. Fate and behavior of oil spilled in the presence of ice—a comparison of the results from recent laboratory, meso-scale flume and field test. Proceedings of the Seventeenth Arctic and Marine Oil Spill Program (AMOP) Technical Seminar, Volume 1. Environment Canada, Ottawa.

Spaulding, M.L., 1988. A state-of-the-art review of oil spill trajectory and fate modelling. *Oil Chemical Pollution*. 4, 39–55.

Spaulding, M.L., 2017. State of the art review and future directions in oil spill modeling. *Marine Pollution Bulletin*. 115, 7–19.

Spaulding, M.L., Howlett, E., Anderson, E., Jayko, K., 1992. OILMAP: a global approach to spill modeling. 15th Arctic and Marine oil Spill Program, Technical Seminar, Edmonton, Alberta, Canada, June 9–11, 1992, pp. 15–21.

Spier, C., Stringfellow, W. T., Hazen, T. C., Conrad, M., 2013. Distribution of hydrocarbons released during the 2010 MC252 oil spill in deep offshore waters . *Environmental Pollution*. 173, 224-230.

Sugioka, S.I., Kojima, T., Nakata, K., Horiguchi, F., 1999. A numerical simulation of an oil spill in Tokyo Bay, *Spill Science & Technology Bulletin*, 5 (1), 51-61.

Sun, Y., Cao, X., Liang, F., 2019. Investigation on underwater spreading characteristics and migrationlaw of oil leakage from damaged submarine pipeline. *Process Safety and Environmental Protection. 127*, 329–347.

Tian, X., Wang, Q., Liu, G., Deng, W., Gao, Z., 2018. Numerical and experimental studies on a three-dimensional numerical wave tank. In: IEEE Access 6. pp. 6585–6593.

Tkalich, P., 2006. A CFD solution of oil spill problems, *Environmental Modelling Software*. 21, 271–282.

Untersteiner, N., Badgley, F. I., 1965. The roughness parameters of sea ice, Journal of Geophysical Research. https://doi.org/10.1029/JZ070i018p04573.

Vankatesh, S., El-Tahan, H., Comfort, G., Abdelnour, R., 1990. Modelling the behavior of oil spills in ice-infested waters. *Atmosphere Ocean*. 28 (3), 303–329.

Wang, J., Shen, Y., 2010. Modeling oil spills transportation in seas based on unstructuredgrid, finite-volume, wave-ocean model. *Ocean Model. 35*, 332–344.

Wang, S.D., Shen, Y.M., Zheng, Y.H., 2005. Two-dimensional numerical simulation for transport and fate of oil spills in seas, *Ocean Engineering*. 32 (13), 1556–1571.

Webler, T., and F. Lord. 2010. Planning for the human dimensions of oil spills and spill response. Environmental Management 45:723-738. http://dx.doi.org/10.1007/s00267-010-9447-9.

Wei, L., Hu, L., Dong, L., Zhao, W., 2014. A damage assessment model of the oil spill accident combining historical data and satellite remote sensing information: A case study in Penglai, 19-3 oil spill accident in China. *Marine Pollution Bulletin*. 91 (1), 258–271.

Wilson, D.G., Mackay, D., 1987. A novel interactive oil spill model. Environment Canada, Conversion and Protection Ottawa 79 90. Proceedings Arctic Marine Oil spill Program Technical Seminar.

Vankatesh, S., El-Tahan, H., Comfort, G., Abdelnour, R., 1990. Modelling the behavior of oil spills in ice-infested waters. *Atmospheric Ocean*. 28 (3), 303–329.

Yang, M., Khan, F., Garaniya, V., Chai, S., 2015. Multimedia fate modeling of oil spills in ice infested waters: an exploration of the feasibility of the fugacity-based approach. *Process Safety and Environmental Protection*. 93, 206–217.

Yao, Y., Huang, G., An, C., Chen, X., Zhang, P., Xin, X., Shen, J. and Agnew, J., 2020. Anaerobic digestion of livestock manure in cold regions: Technological advancements and global impacts. *Renewable and Sustainable Energy Reviews*. 119, 109494.

Yapa, P.D., Dasanayaka, L.K., Bandara, U.C., Nakata, K., 2010. A model to simulate the transportand fate of gas and hydrates released in deepwater. *Journal of Hydraulic Research. 48 (5)*, 559–572.

Yapa, P.D., Weerasuriya, S.A., 1997. Spreading of oil spilled under floating broken ice. *Journal of Hydraulic Engineering* 123 (8), 676–683.

Yumashev, D., van Hussen, K., Gille, J., Whiteman, G., 2017. Towards a balanced view of Arctic shipping: estimating economic impacts of emissions from increased traffic on the Northern Sea route. *Climate Chang*. 143 (1–2), 143–155.

Zelenke, B., O'Connor, C., Barker, C., Beegle-Krause, C.J., Eclipse, L. (Eds.), 2012. General NOAA Operational Modeling Environment (GNOME) Technical Documentation. U.S. Dept. of Commerce, NOAA Technical Memorandum NOS OR&R 40. Seattle, WA: Emergency Response Division, NOAA, p. 105 (PDF version, 2MB; Word version, 2.5 MB).

Zhang, Z., Li, S.S., 2017. Large eddy simulation of rough surface turbulent flow in open channel. *25th Annual CFDSC Conference.* Windsor, ON, Canada.

Zhao, S., Huang, W.W., Wang, X.Q., Fan, Y.R. and An, C.J., 2019. Sorption of phenanthrene onto diatomite under the influences of solution chemistry: A study of linear sorption based on maximal information coefficient. . *Journal of Environmental Informatics*. 34(1). 35-44.

Zheng, L., Yapa, P.D., Chen, F.H., 2003. A model for simulating deepwater oil and gas blowoutspart I: theory and model formulation. *Journal of Hydraulic Research. 41 (4)*, 339–351.

Zhu, H., Lin, P., Pan, Q., 2014. A CFD (computational fluid dynamic) simulation for oil leakage from. *Energy. 64*, 887-899.

Zhu, H., You, J., Zhao, H., 2017. Underwater spreading and surface drifting of oil spilled from asubmarine pipeline under the combined action of wave and current. *Applied Ocean Research. 64*, 217-235.

Zhu, Z., Zhang, B., Cai, Q., Ling, J., Lee, K., & Chen, B., 2020. Fish waste based lipopeptide production and the potential application as a bio-dispersant for oil spill control. *Frontiers in Bioengineering and Biotechnology*. 8, 734.